

1 | **Title:** ~~Low-P, high-T metamorphic~~ overprint in ultramafic and mafic  
2 | eclogite-facies rocks of the Central Alps: clues from srilankite ( $ZrTi_2O_6$ )- and spinel ±  
3 | sapphirine ± corundum-bearing symplectites

Formattato: Pedice

Formattato: Pedice

5 | Running title: ~~LP~~-HT overprint in eclogites from Central Alps

7 | Simone Tumiati<sup>(1,\*)</sup>, Stefano Zanchetta<sup>(2)</sup>, Luca Pellegrino<sup>(2)</sup>, Claudia Ferrario<sup>(1)</sup>, Stefano  
8 | Casartelli<sup>(1)</sup>, Nadia Malaspina<sup>(2)</sup>

Formattato: Apice

10 | (1) Dipartimento di Scienze della Terra, Università degli Studi di Milano  
11 | Via Mangiagalli 34, 20133 – MILANO (Italy)

12 | (2) Dipartimento di Scienze dell'Ambiente e della Terra, Università degli Studi di Milano  
13 | Bicocca. Piazza della Scienza 4, 20126 – MILANO (Italy)

15 | \*Corresponding author: Phone: +39-0250315625; FAX: +39-0250315597; E-mail:  
16 | simone.tumiati@unimi.it

18 | **Key words:** Duria, granulite, peridotite, geothermobarometry, zirconium

20 | **Abstract: max 300 words no abbreviations and citations**

21 | Eclogite-facies garnet peridotites and different types of eclogites with a broadly MORB  
22 | signature ~~erop out~~ around Monte Duria (Italy) ~~in the~~ Adula nappe of the Central Alps)  
23 | ~~display -~~High-pressure peaks at ~~P, P =~~ 2.6–3.09 GPa and ~~T, T =~~ 860–720–740–900 °C for  
24 | peridotites, and ~~at P, P =~~ 2.8–3.0 GPa ~~2.5~~ and ~~T, T =~~ 720–700–740 °C for eclogites, ~~have~~  
25 | ~~been~~ retrieved by conventional thermobarometry, ~~and~~ thermodynamic modelling ~~and on the~~  
26 | ~~basis of the presence in eclogites of pargasite and K feldspar~~. High-pressure minerals are  
27 | replaced both in peridotites and in eclogites by lower ~~er~~-P, high-T assemblages. In peridotites,  
28 | ~~the zirconium titanate~~ srilankite ( $Zr_{0.33}Ti_{0.66}O_2$ ) occurs as  $\mu$ m-sized crystals in textural  
29 | equilibrium with spinel, clinopyroxene and orthopyroxene in coronas and symplectites  
30 | surrounding ~~garnet~~ olivine. By using a new  $ZrO_2$ - $TiO_2$  ~~solid-solid~~ solution model, we  
31 | ~~interpreted evidence~~ that srilankite ~~has formed after~~ is stable in peridotites against zircon +  
32 | rutile ~~at T, T =~~ 900–800 °C ~~at P ≈~~ 1.0 GPa, ~~which is consistent with T =~~ 850 °C ~~P, T at P =~~  
33 | 1.58 GPa ~~estimateds by conventional thermobarometry or~~ for symplectites replacing garnet  
34 | ~~bearing ie phases~~ sapphirine + spinel + orthopyroxene + amphibole ( $T \approx 850$  °C at 1.0 GPa);

Formattato: Tipo di carattere:  
Corsivo

Formattato: Tipo di carattere:  
Corsivo

Formattato: Tipo di carattere:  
Corsivo

Formattato: Tipo di carattere:  
Corsivo

Formattato: Tipo di carattere:  
Corsivo

Formattato: Tipo di carattere:  
Corsivo

Formattato: Tipo di carattere:  
Corsivo

Formattato: Tipo di carattere:  
Corsivo

Formattato: Tipo di carattere:  
Corsivo

35 In eclogites, ~~high P phases~~ kyanite ~~and zoisite are~~ replaced by symplectites made of  
36 anorthite-rich plagioclase + spinel  $\pm$  ~~Al-rich~~ peraluminous sapphirine  $\pm$  corundum.  
37 Thermobarometry suggests that these symplectites formed at ~~T, T  $\approx$  850°C~~ ~~at and P, P =~~  
38 ~~10.80–1.02~~ GPa, conditions which are ~~similar coincident~~ to the ~~low P~~, high-~~T~~ overprint  
39 observed in peridotites. Thermodynamic modelling coupled with a material-transfer study  
40 suggests that at these ~~P, T, P, T~~ conditions corundum and sapphirine are stable only in the  
41 ~~micro-domain surrounding pseudomorphs after~~ kyanite ~~and zoisite~~, resulting from the local  
42 ~~enrichment high content~~ in aluminium ~~of these micro-domains~~, which could not fully  
43 equilibrate with the surrounding rock due to the "inert" character of this component (~~i.e.~~,  
44 ~~mosaic equilibrium~~). This is the first report of eclogite-facies rocks showing a ~~LP~~-  
45 ~~HT~~ granulite-facies metamorphic overprint in the Central Alps, ~~which is instead well~~  
46 ~~documented in other pre-Alpine complexes~~. On these basis, alternative than available models  
47 are needed to explain the subduction-exhumation evolution of garnet peridotites and hosting  
48 eclogites of the Adula-Cima Lunga unit.

Formattato: Tipo di carattere:  
Corsivo

Formattato: Tipo di carattere:  
Corsivo

Formattato: Tipo di carattere:  
Corsivo

Formattato: Tipo di carattere:  
Corsivo

Formattato: Tipo di carattere:  
Corsivo

## 50 INTRODUCTION

51 Outcrops of eclogite-facies rocks showing granulite-facies overprint are worldwide  
52 restricted to a few localities. These rocks often show spectacular examples of metamorphic  
53 reactions, where relicts of high-pressure (HP) minerals are partially replaced by ~~low pressure~~  
54 (~~LP~~), high-temperature (HT) ~~symplectitic~~ assemblages (~~e.g.~~, ~~(Morishita et al., 2001;~~  
55 Nakamura and Hirajima, 2000; Scott et al., 2013), ~~commonly forming symplectitic~~  
56 ~~intergrowths~~). The study of these symplectites is not always straightforward, because of the  
57 tiny dimension of the phases and the possible differences in bulk composition between the  
58 symplectite micro-domain and the surrounding rock due to variable element mobility and the  
59 opening of the system (~~e.g.~~, ~~(Godard and Mabit, 1998; Godard and Martin, 2000)~~).  
60 Nevertheless, their understanding can provide unrivalled records of the eclogite-granulite-  
61 facies transition.

62 ~~LP-HT~~ spinel + orthopyroxene + clinopyroxene symplectites (kelyphites) surrounding  
63 HP garnet in deep mantle peridotites are relatively common and similar, resulting from the  
64 ~~LP-HT~~ retrograde reaction between garnet and olivine (see review of Godard & Martin, 2000).  
65 In the Alps, ~~nice~~ examples can be found in garnet peridotites from the Central Alps (Adula-  
66 Cima Lunga unit) and the Eastern Alps (Ulten zone, ~~)~~ (see review of ~~(Morten and~~  
67 Trommsdorff, ~~2003)~~).

68 ~~LP~~-HT overprint in eclogites can lead to complex assemblages, varying in function of the

69 bulk chemistry and the availability of fluids. In kyanite-bearing eclogites, spinel ± corundum  
70 ± sapphirine symplectites have been described in different granulite terranes from the  
71 Precambrian to the Caledonides and the Variscides (Baldwin *et al.*, 2007; Carswell *et al.*,  
72 1989; Johansson and Möller, 1986; Liati and Seidel, 1996); O'Brien, 1992; Godard & Mabit,  
73 1998; Möller, 1999).

74 Here we present an integrated approach to study the LP-HT overprint on garnet  
75 peridotites and different types of eclogites cropping out in the Duria area in the southern part  
76 of the Adula Nappe in the Central Alps. In particular, we focused on: i) ~~a rare~~ Zr-bearing  
77 symplectites containing the zirconium titanate srilankite (Zr,Ti)<sub>2</sub>O<sub>64</sub>; ii) ~~sapphirine + spinel-~~  
78 bearing symplectites replacing garnet occurring in garnet peridotite; iii) spinel ± sapphirine ±  
79 corundum-bearing symplectites replacing kyanite ~~and zoisite occurring~~ in eclogites.

80 Thermodynamic modelling of Zr-bearing symplectites in peridotites has been accomplished  
81 by developing a new binary solution model between ZrO<sub>2</sub> (baddeleyite) and TiO<sub>2</sub> (rutile) with  
82 the intermediate compound srilankite, calibrated against published experimental data at high-  
83 pressure conditions. A ~~material-material~~ transfer study has been performed by calculating ~~P-~~  
84 ~~T-X~~ and ~~aH<sub>2</sub>O-X~~ phase diagrams to ~~address assess the stability of~~ spinel, sapphirine and  
85 corundum in symplectites replacing garnet (in peridotite) and kyanite (in eclogite). ~~and zoisite~~  
86 ~~in eclogites.~~ The integration of conventional thermobarometry, thermodynamic modelling and  
87 ~~material-material~~ transfer study allowed to retrieve the petrological processes that occurred in  
88 these rocks from the eclogite to the ~~granulite granulite~~-facies transition, and to provide new ~~P-~~  
89 ~~T~~ estimates of the eclogite-facies peak and the LP-HT granulite-facies  
90 metamorphism metamorphic overprint, which are discussed in the framework of the pre-  
91 Alpine and Alpine metamorphism of this polycyclic basement.

## 93 GEOLOGICAL SETTING

94 The Adula-Cima Lunga nappe complex is located on the eastern flank of the Lepontine  
95 Dome (Fig. 1) and it represents the highest of the ~~so-called~~ Lower Penninic units of the  
96 Central Alps (e.g. (Milnes, 1974; Schmid *et al.*, 1996). Its position in the Central Alps edifice  
97 is comprised between the ~~Lower Penninic~~-nappe stack formed by the Leventina-Lucomagno  
98 (L-L); Maggia and Simano (Sm) units at the bottom, and the Middle Penninic units at the top  
99 (Tambo units, Chiavenna metaophiolites and Suretta unit, (Maggia – Mg, Tambo – Tb,  
100 Suretta – Su; Fig.1). The contact with the Middle Penninic nappes occurs along the Misox  
101 Zone, a thin unit made of metasediments, MORB-derived amphibolites and slivers of  
102 continental basement ((Steinmann and Stille, 1999; Stucki *et al.*, 2003). The lower contact of

Formattato: Pedice

Formattato: Tipo di carattere:  
Corsivo

Formattato: Tipo di carattere:  
Corsivo

Formattato: Tipo di carattere:  
Corsivo

Formattato: Tipo di carattere:  
Corsivo

Formattato: Tipo di carattere:  
Corsivo

Formattato: Tipo di carattere:  
Corsivo

103 the Adula nappe is somewhat less defined due do lithological similarities with the Simano  
104 gneiss and the Tertiary ~~high-high~~-grade metamorphism of the Lepontine Dome that  
105 overprinted existing tectonic structures (Nagel, 2008). To the south, a lithologically  
106 heterogeneous E-W trending zone, namely the Southern Step Belt (SSB) or Bellinzona-  
107 Dascio Zone (Schmid *et al.*, 1996), is interposed between the Adula nappe and the western  
108 tail of the Bergell pluton, ~~which is dextrally displaced along the Insubric Fault~~ (Fig. 1). To the  
109 ~~e~~East, the Gruf Complex, considered part of the Adula nappe ((Berger *et al.*, 2005), ~~but see~~  
110 ~~(Galli *et al.*, 2013) for alternative interpretation~~), is separated from the main units of the nappe  
111 complex by the Forcola normal fault (Ciancaleoni and Marquer, 2006). It is worth noting here  
112 that the interpretation of the Gruf Complex as pertaining to the Adula Nappe has been  
113 recently challenged by Galli *et al.* (2013), who suggest a pre-Alpine history for this complex.

114 The Adula nappe largely consists of orthogneiss and paragneiss of pre-Mesozoic origin  
115 (Frey and Ferreiro-Mählmann, 1999; Liati *et al.*, 2009; Rubatto *et al.*, 2009), variably  
116 retrogressed eclogites preserved as boudins within paragneiss, minor ultramafic bodies and  
117 metasedimentary rocks of presumed Mesozoic age (Galster *et al.*, 2012), with references), the  
118 latter chiefly preserved in the middle and northern domains of the nappe.

119 Paleogeographic reconstructions locate the Adula nappe in the former distal European  
120 margin (Schmid *et al.*, 1990), to the north of the North Penninic Ocean, opened since the  
121 Jurassic and later closed during the Late Cretaceous-Eocene phase of ~~-~~convergence between  
122 Europe and Africa-Adria (Dewey *et al.*, 1989).

123 During the Tertiary Alpine orogenic cycle the Adula nappe and the crustal slivers that now  
124 made the SSB, were subducted to mantle depths (Becker, 1993; Evans and Trommsdorff,  
125 1978; Gebauer, 1996; Heinrich, 1986). Metamorphic conditions at peak pressure are found to  
126 increase southward, from  $\approx 1.7$  GPa and  $\approx 650^\circ\text{C}$  in the north, to  $2.5\text{--}3.0$  GPa and  $\approx$   
127  $750^\circ\text{C}$  in the south (Brouwer *et al.*, 2005; Dale and Holland, 2003).

128 Even more severe ~~higher~~-conditions have been estimated for the peridotite and  
129 metaperidotite lenses that occur at the southern, western and eastern margins of the nappe  
130 (Fumasoli, 1974; Pfiffner and Trommsdorff, 1998). Garnet lherzolite bodies crop out at three  
131 localities, from west to east: Cima di Gagnone, Alpe Arami and Monte Duria (Fig. 1). Such  
132 mantle-derived rocks equilibrated at pressure ~~in excess~~ of  $\approx 3.0$  GPa and temperature of 800-  
133  $850^\circ\text{C}$  (e.g. (Hermann *et al.*, 2006; Nimis and Trommsdorff, 2001).

134 An older ~~high~~-high-pressure event of Variscan age (Herwartz *et al.*, 2011; Liati *et al.*,  
135 2009) is seldom preserved within eclogitic boudins of the central and northern sector of the  
136 Adula nappe.

137 After the partial subduction of the European distal margin beneath the ~~Africa~~-Adria  
138 margin, the ~~high~~-high-pressure rocks of the Adula nappe and the SSB were overprinted by an  
139 upper ~~amphibolite~~-~~amphibolite~~-facies metamorphism (Todd and Engi, 1997; Wenk, 1970),  
140 ~~which that~~-postdates the main phase of nappe-stacking. In the southern sector of the  
141 Lepontine Dome, adjacent to the Insubric Fault (Fig. 1), metamorphic conditions promoted  
142 extensive migmatization of both metasedimentary and metagranitoid rocks (“Migmatite  
143 belt”~~;~~ (Burri *et al.*, 2005)). Partial melting occurred in the 32-22 time interval (Rubatto *et al.*,  
144 2009) and was promoted essentially by fluid-present processes (Berger *et al.*, 2008), whereas  
145 fluid-absent melting of white mica was restricted to a narrow zone between Bellinzona and  
146 Lake Como (Fig. 1) in the Adula nappe and the SSB (Burri *et al.*, 2005).

147

#### 148 **Field aspects of peridotites and hosting crustal rocks**

149 Two sites of the Duria area have been investigated in detail: (i) the outcrop of Borgo and  
150 (ii) outcrops within sight to Monte Duria (Figs. 1, 2).

151 At Borgo (Fig. 2), a hm-sized peridotite body is in contact with amphibole-bearing  
152 migmatites with preserved boudins of mafic eclogites. The peridotite body and its mafic rocks  
153 rim are hosted within migmatitic gneisses, like those hosting peridotites at Monte Duria (Fig.  
154 2). In the peridotite body, garnet was not observed (~~Fig. 3a,b~~), but rounded chlorite-rich  
155 pseudomorphs that likely formed after garnet porphyroclasts are abundant; ~~1-4~~~~mm~~- to cm-  
156 sized garnet (up to 3 cm), often partially replaced by chlorite and/or kelyphite, has been found  
157 ~~downstream~~ in close-by loose blocks ~~on downstream in~~ the Rio Ledù stream bed (Fig. 3\_a). In  
158 the Borgo body, a compositional layering marked by chlorite-rich and chlorite-poor layers  
159 represents the main fabric element at the mesoscale (Fig. 3\_b). Such layering is locally  
160 transposed by a second foliation marked by chlorite. The contact between the peridotite and  
161 hosting crustal rocks is characterized by the occurrence of ~~a few decimeters~~-~~decimeter~~-thick  
162 metasomatic rim rich in amphibole (amph) and phlogopite (phl). Lenses rich in amph + phl  
163 have been also found as cm-sized boudins embedded in the surrounding mafic rock (Fig. 2).  
164 A phl-rich pegmatite intruded the peridotite-mafic rocks contact and is folded together with  
165 chlorite-~~defined~~ foliation in the peridotite and the main foliation of hosting mafic gneiss. -The  
166 heterogeneous rocks association that ~~make~~~~s~~ the rim of the peridotite body consists chiefly  
167 of amphibole-bearing migmatitic gneiss (AG in Fig. 2) with boudins of mafic rocks (Fig. 2,  
168 3c, 3d) that show differences in terms of mineralogical composition and deformation. Fine  
169 grained, partially retrogressed, dark green eclogites (ME in Fig. 2) occur as boudins (dm to m  
170 in size, Fig. 3c) included in plagioclase (pl)- and amphibole-rich gneisses. A second type of

171 | eclogite occurs in larger light-green ~~colored~~ boudins (Fig. 2 and 3d). The contact between the  
172 | second type eclogites (E in Fig. 2) and surrounding pl+amph gneisses is locally marked by  
173 | mm-sized layers (Fig. 3e, HAE in Fig. 2), where cm-sized crystals of emerald-green zoisite  
174 | surrounded by reddish coronae have been found (Fig. 3f).

175 | On the southeast ridge of Monte Duria, about 250 m from the summit (Fig. 1), several  
176 | scattered peridotite bodies (Fig. 3g) occur within migmatitic gneisses (Fumasoli, 1974).  
177 | Peridotites are often garnet-bearing, although garnet (gt) (mm- to cm-sized) is invariably  
178 | surrounded by symplectitic intergrowths ("kelyphite", Fig. 3h; cf. Godard and Martin, 2000)  
179 | and commonly retrogressed to pseudomorphic assemblages. Orthopyroxene (opx) and  
180 | emerald-green clinopyroxene (cpx) ~~are often visible~~ occur often as mm- to cm-sized ~~crystals~~  
181 | ~~embedded in an oriented porphyroclasts~~ in an oriented dark fine-grained olivine matrix. Cpx ±  
182 | gt-rich veins cut at places these peridotite bodies.

183 | The peridotite lenses commonly display a strongly foliated rim (Fig. 3h3g), with a chlorite  
184 | foliation parallel to the main foliation of hosting gneisses, and a core where a compositional  
185 | layering with gt- rich and gt-poor levels occur.

186 |

## 187 | MATERIALS AND METHODS

188 | ~~More than 50 thin sections of rocks from the Duria area have been analysed at the~~  
189 | ~~petrographic and scanning electron microscopes. For this study, we selected 12 rocks,~~  
190 | ~~representative of peridotite and mafic rocks cropping out at Monte Duria and Borgo.~~

191 | Major-elements whole-rock analysis was performed by inductively-coupled plasma mass  
192 | spectrometry (ICP-MS) and LECO combustion analysis (total C, S) (Bureau Veritas ACME  
193 | Mineral Laboratories, Canada). Bulk-rock chemistry has been evaluated ~~by using bivariate~~  
194 | ~~plots (supplementary Fig. SM 1) and using the~~ principal component analysis (~~supplementary~~  
195 | ~~Fig. SM 2)PCA). In particular, this method was used to classify mafic rocks in groups~~  
196 | ~~showing similar element correlation. PCA is a statistical procedure that transforms a number~~  
197 | ~~of possibly correlated variables into the same number of uncorrelated variables given by the~~  
198 | ~~eigenvectors of the covariance matrix, and called principal components. The first principal~~  
199 | ~~component (F1) account for as much of the variability in the data as possible, and thus~~  
200 | ~~corresponds to the highest eigenvalue of the covariance matrix; each of the succeeding~~  
201 | ~~components (F2, F3...) accounts for as much of the remaining variability as possible. For~~  
202 | ~~other details and examples of PCA applied to geosciences, refer for instance to (Tumiati *et al.*,~~  
203 | ~~2005, 2008, 2010, 2013).~~

204 Quantitative analyses of minerals were performed using a JEOL 8200 wavelength-  
205 dispersive electron microprobe (EMP), at 15-kV accelerating potential, 5-nA sample current  
206 and 1- $\mu$ m beam diameter. Standards used were omphacite (Na), grossular (Ca, Al and Si),  
207 fayalite (Fe), olivine (Mg), orthoclase (K), rhodonite (Mn), ilmenite (Ti), niccolite (Ni), pure  
208 Cr (Cr) and zircon (Zr, Hf). A counting time of 30 s was applied for all elements. [Ti traces in  
209 quartz and Zr traces in rutile have been measured at 15-kV accelerating potential and 100-nA  
210 sample current, with a counting time of 300 s \(150 s for background\). Hf traces in  \$\mu\$ m-sized  
211 zircon, srilankite and baddeleyite in peridotite have been measured at 15-kV accelerating  
212 potential and 5-nA sample current \(15 nA for larger zircon crystals in eclogite\), with a  
213 counting time of 300 s \(150 s for background\).](#) The  $\text{Fe}^{3+}/\text{Fe}_{\text{TOT}}$  ratio in minerals [reported in  
214 Table 2](#) has been calculated by stoichiometry. [Cathodoluminescence images of quartz has  
215 been collected at 15-kV accelerating potential and 100-nA sample current.](#)

216 Thermodynamic modelling has been performed using the software package Perple\_X  
217 (<http://www.perplex.ethz.ch>; Connolly, 2005), using the thermodynamic database of  
218 Holland and Powell, (1998) revised to 2002 (hp02ver.dat), and the following solution  
219 models, [described in](#) Holland and Powell, (1998) (HP), Diener-HENER and POWELL-Powell,  
220 (2012) (GHP2), Holland and Powell, (2003) (H,HP), and Dale *et al.*, (2000) (DHP): Gt(HP)  
221 for garnet, Opx(HP) for orthopyroxene, O(HP) for olivine, [Cpx\(HP\) for clinopyroxene,  
222 Chl\(HP\) for chlorite, Sp\(HP\) for spinel, Pheng\(HP\) for white mica, Sapp\(HP\) for sapphirine,  
223 Omph\(GHP2\) for ~~clinopyroxene~~omphacite, Pl\(H,HP\) for ternary feldspars, ~~Sp\(HP\) for  
224 spinel, Pheng\(HP\) for white mica,~~ Amph\(DHP\) for amphibole, ~~and Sapp\(HP\) for  
225 sapphirine~~ and the water equation of state of Holland and Powell \(1998\). Thermodynamic  
226 modelling of Zr-bearing systems was accomplished first by creating the ordered srilankite  
227 end-member as a linear combination of 2/3 rutile \( \$\text{TiO}\_2\$ \) and 1/3 baddeleyite \( \$\text{ZrO}\_2\$ \). \[The  
228 srilankite Gibbs free energy of formation was corrected according to\]\(#\) Cancarevic \*et al.\*,  
229 \(2006\). \[A ~~The~~ baddeleyite-srilankite-rutile solution model was then presented in this  
230 study is\]\(#\) calibrated against the experimental data of Troitzsch \*et al.\*, \(2004\) and TOMKINS  
231 Tomkins \*et al.\*, \(2007\) at 2 GPa \[and 800–1200° C\]\(#\). Retrieved activity-composition relations  
232 are expressed according to the van Laar formulation \(Holland & Powell, 2003\), which allows  
233 describing asymmetrical miscibility gaps. \[Other details about the solid solution model are  
234 provided as Supplementary Information.\]\(#\)](#)

235

236 **PETROGRAPHY, BULK-ROCK CHEMISTRY AND MINERAL CHEMISTRY OF**  
237 **DURIA ROCKS**

238

## 239 **Garnet peridotites**

240 Garnet-bearing peridotites from the Duria area have been sampled from: i) one of the  
241 several migmatite-hosted boudins occurring close to Monte Duria (A2C2, [MD20 and MD25](#)  
242 in Table 1 [and 2](#)); ii) loose blocks found downstream in the Rio Ledù stream bed cutting the  
243 Borgo outcrop (B1 and B3A [in Table 1 and 2](#)). Borgo peridotites are indistinguishable from  
244 the peridotite of Monte Duria in terms of microtexture, mineral assemblage and bulk-  
245 rock/mineral chemistry. Slight variations in SiO<sub>2</sub>, CaO, Al<sub>2</sub>O<sub>3</sub> (Table 1) are imputable to  
246 differences in modal proportion of cpx, gt and opx.

247 Garnet-bearing peridotites are composed by more than 90 vol% of polygonal olivine (100-  
248 200 μm), partially serpentinised especially along late fractures (Fig. 4a,b,c). The occurrence  
249 of serpentine accounts for the relatively high bulk loss-on-ignition (LOI) (Table 1). The XMg  
250 (=Mg/Fe+Mg) of olivine is 0.89-0.91 (Table 2), comparable to the bulk rock XMg = 0.90.  
251 Minor phases are clinopyroxene (cpx), orthopyroxene (opx), garnet, spinel (sp), amphibole  
252 and accessory ilmenite, pyrrhotite and pentlandite. In sample A2C2, we observed tiny crystals  
253 (~1 μm) of srilankite (Zr<sub>0.33</sub>Ti<sub>0.66</sub>O<sub>2</sub>) ~~and a single crystal of baddeleyite (Zr<sub>0.99</sub>Ti<sub>0.01</sub>O<sub>2</sub>)~~ in a  
254 double coronas formed at the contact between olivine and garnet (Fig. 5a). ~~These Zr~~  
255 ~~phases~~ [Srilankite](#) occur [both](#) in the opx corona replacing the former olivine ([Fig. 5b](#)) and in the  
256 ~~opx+ cpx + sp opx+cpx+sp crystals in~~ kelyphite replacing garnet ([Fig. 5 d](#)). In this latter  
257 intergrowth, we found also [few](#) crystals of zircon [and baddeleyite \(Zr<sub>0.99</sub>Ti<sub>0.01</sub>O<sub>2</sub>\)](#) ([Fig. 5 c. e. ,](#)  
258 [f](#)). [The Hf content in zircon, srilankite and baddeleyite is highly scattered \(Table 3\).](#)  
259 [Maximum contents are 0.72 wt% HfO<sub>2</sub> in baddeleyite \[Hf/\(Zr+Hf\) = 0.005\], 0.40 wt% HfO<sub>2</sub>](#)  
260 [in srilankite \[Hf/\(Zr+Hf\) = 0.007\] and 0.05 wt% HfO<sub>2</sub> in zircon \[Hf/\(Zr+Hf\) = 0.001\].](#)

Formattato: Pedice

261 Gt occurs as porphyroblasts and porphyroclasts of variable size up to 3 cm ([Fig. 4 a, c; Fig.](#)  
262 [6 a](#)). It is [only](#) slightly zoned from core to rim ([supplementary figure SM3](#)), ~~with displaying~~  
263 [an](#) average XMg = 0.80-79 (Py<sub>6870</sub>Alm<sub>197</sub>Gr<sub>9</sub>Uv<sub>413</sub>) in the core and [an](#) average XMg = 0.767  
264 (Py<sub>667</sub>Alm<sub>210</sub>Gr<sub>9</sub>Uv<sub>413</sub>) ~~in the rim in the rim, with Cr content up to 2.49 wt% Cr<sub>2</sub>O<sub>3</sub> (0.14~~  
265 ~~a.p.f.u.).~~ [In samples MD20 and MD25, symplectites developed along fractures in garnet](#)  
266 [contain sapphirine, in textural equilibrium with spinel, orthopyroxene and amphibole \(Fig.](#)  
267 [7a\). Sapphirine is characterised by XMg = 0.93–0.95 and is Al-rich \(17.36–17.61 a.p.u.f. on a](#)  
268 [basis of 28 cations\), close to the sapphirine end-member \(7 : 9 : 3\).](#)

Formattato: Non Apice / Pedice

Formattato: Pedice

Formattato: Non Apice / Pedice

269 Cpx, opx, sp and amph occurs as mm- to cm-sized porphyroclasts, found both in the matrix  
270 ([Fig. 4 b; Fig. 6 a](#)) and included in garnet, and ~~as fine-grained kelyphite in coronas~~  
271 surrounding garnet ([Fig. 4 c; Fig. 5b6 a](#)).



272 Porphyroclastic cpx is diopside-rich with XMg = 0.95, Cr up to 0.04 a.p.f.u. and jadeite  
273 content up to 7%. Cpx in kelyphite displays negligible jadeite contents and higher Al (0.018  
274 a.p.f.u.). In sample B3,  $\mu\text{m}$ -sized inclusions of edenitic amphibole (XMg = 0.94) and dolomite  
275  $(\text{Ca}_{1.01}\text{Mg}_{0.94}\text{Fe}_{0.05})(\text{CO}_3)_2$  have been observed in cpx porphyroclasts.

276 Porphyroclastic opx is enstatite rich (XMg = 0.92) and Al poor (0.03 a.p.f.u.), while opx  
277 and in the kelyphitic assemblage becomes richer in Fe (XMg = 0.89–0.92) and Al (up to 0.08  
278 a.p.f.u. in sapphirine-free symplectites; up to 0.20 a.p.f.u. in sapphirine-bearing symplectites)  
279 (Table 2) in the kelyphitic assemblage.

280 Primary spinel occurs both as porphyroclasts in the matrix (Fig. 6 a) and rarely included  
281 in garnet. Often, former spinel inclusions in garnet are now embedded in kelyphites, which  
282 contain a second generation of spinel forming vermicular intergrowths with opx and cpx.  
283 Spinel composition shows dramatic variations, being spinel porphyroclasts and inclusions rich  
284 in Fe (XMg = 0.47) and Cr (Cr/Al+Cr = 0.56), especially at the core, while kelyphitic  
285 symplectitic spinel and rims of spinel porphyroclasts are Fe poor (XMg = 0.76–0.84) and Cr  
286 poor (Cr/Al+Cr = 0.04) (Fig. SM 3 b).

287 Amphibole porphyroclasts are pargasitic to edenitic in composition, while kelyphitic  
288 amphibole is tschermakite to magnesiohornblende. In sample B3A, we observed a late  
289 generation of kelyphitic intergrowth composed of chlorite, anthophyllite and phlogopite.

290

## 291 Mafic rocks

292 Mafic rocks were sampled systematically in the Borgo outcrop, where these rocks are in  
293 contact with peridotites (Figs. 2, 3). The different types of mafic rocks are not easy to  
294 distinguish in the field. Therefore, these rocks have been classified on the basis of their  
295 bulk-rock chemistry (Table 1) and petrographic features described below. In particular, the  
296 principal component analysis (PCA) has been applied in order to identify groups of rocks  
297 showing similar element correlation (Fig. 6). Overall, As a general consideration, the  
298 compositions of the Borgo mafic rocks are broadly comparable ascribable to N-MORB  
299 basalts gabbros showing various degrees of differentiation (cf. Klein, 2003), showing resulting  
300 in variable XMg (from 0.61 to 0.84), and  $\text{Al}_2\text{O}_3$  (from 14.61 to 20.83 wt%), CaO (from 9.57  
301 to 13.24 wt%) and  $\text{TiO}_2$  (from 0.16 to 1.65 wt%) contents (supplementary Fig. 1). A more  
302 detailed characterization of these rocks is beyond the purpose of this paper and will be given  
303 elsewhere. In this study, the principal component analysis (PCA) has been applied in order to  
304 identify groups of rocks showing similar element correlation (supplementary Fig. SM 2).

Formattato: Non Evidenziato

Formattato: Non Evidenziato

Formattato: Pedice

305 PCA distinguishes among mafic rocks: i) kyanite eclogites (E)<sub>2</sub> samples D3 and B5,  
306 showing ~~anthe lowest covariance average content~~ for all elements; ii) mafic eclogites (ME)<sub>2</sub>  
307 samples D6 and D4, showing the highest contents in Fe, Ti, ~~P, P~~ and Mn (dark green on the  
308 field); iii) high-Al eclogites (HAE)<sub>2</sub> samples D1, D8 and D9, showing the highest contents in  
309 Al, Si, Na and K; iv) pl+amph gneisses (AG)<sub>2</sub> samples D5 and D2, showing the highest  
310 contents in Ca and Cr. The mineralogy and petrography of these lithotypes is provided below.

311

### 312 *Kyanite eclogites (E)*

313 In these rocks, a symplectitic matrix composed of diopside-rich ~~and jadeite-poor~~  
314 clinopyroxene (~~Di<sub>81</sub>Hed<sub>15</sub>Jd<sub>6</sub> XMg = 0.87-0.88~~) and albite-rich plagioclase (up to ~~Ab<sub>73</sub>Ab<sub>43</sub>~~) is  
315 dominant ([Table 2](#); [Fig. 4e6b](#); [Fig. 75b,ce](#)). In sample D3, these symplectites appear as  
316 pseudomorphs after former mm-sized stubby prismatic crystals embedded in quartz,  
317 ~~associated to Ca-rich plagioclase pseudomorphs likely after zoisite (Fig. 7f; see also eclogites~~  
318 ~~HAE below)~~. The average ~~bulk~~ composition of a representative ~~cpx + pl~~ symplectite has been  
319 measured by averaging 400 EMP analyses (1  $\mu\text{m}$  step) over a  $20\ \mu\text{m} \times 20\ \mu\text{m}$  area, and it  
320 ~~would~~ corresponds to a ~~mixed composition between quartz and to a mixed composition of~~  
321 ~~83.7 mol% omphacitic clinopyroxene Di<sub>58</sub>Jd<sub>32</sub>Hd<sub>10</sub> and 16.3 mol% quartz, strongly~~  
322 ~~suggesting that symplectites formed due to the reaction Ab (in pl) = Jd (in cpx) + qtz~~  
323 (Holland, 1980). ~~A It is noteworthy that ffew~~ inclusions of relict omphacite have been  
324 observed in ~~a~~ kyanite ([Fig. 6c](#)) and garnet porphyroclasts ([Fig. 5d](#)) in sample ~~B5~~, displaying  
325 an almost identical composition Di<sub>58</sub>Jd<sub>33</sub>Hd<sub>9</sub> ([Table 2](#)). Other porphyroclasts consist of  
326 ~~slightly zoned homogeneous~~ garnet (core: Py<sub>3841</sub>Alm<sub>3736</sub>Gr<sub>24</sub>Sp<sub>1</sub>; rim: Alm<sub>42</sub>Pv<sub>35</sub>Gr<sub>20</sub>Sp<sub>2</sub>; see  
327 ~~also supplementary Fig. SM 4 a, b<sub>2</sub>~~), quartz, ~~K-feldspar (Or<sub>97-98</sub> in sample D3) and~~ pargasitic  
328 amphibole (XMg = 0.82) ([Fig. 5e6b](#)) and ~~K-feldspar (Or<sub>97-98</sub>) in sample D3~~.  
329 ~~Cathodoluminescence images of monocrystalline quartz revealed a grain core showing a~~  
330 ~~peculiar layered zonation, resembling twinning planes of a former phase surrounded by a~~  
331 ~~polycrystalline rim (Fig. 6 d), now fully recovered~~. Rutile is an accessory mineral, commonly  
332 found included in garnet and kyanite porphyroclasts. Other accessory phases are ilmenite  
333 (replacing rutile ~~in symplectites~~), zircon and apatite. ~~Traces of Zr in rutile included in garnet,~~  
334 ~~and of Ti in porphyroclastic quartz have been measured for thermometric purposes and will~~  
335 ~~be given in the next Section~~. Garnet and kyanite are typically replaced by symplectitic  
336 intergrowths ([Fig. 7 b, c5e](#)). Symplectites surrounding garnet ([Fig. 4e,f](#)) usually consist of  
337 plagioclase and magnesiohornblende, although relict symplectites containing orthopyroxene  
338 (XMg = 0.74; [Table 2](#)) and plagioclase have been observed ([Fig. 7 b](#)). Symplectites

Formattato: Tipo di carattere:  
Corsivo

Formattato: Tipo di carattere:  
Corsivo

Formattato: Pedice

Formattato: Pedice

Formattato: Pedice

Formattato: Non Apice / Pedice

Formattato: Non Apice / Pedice

Formattato: Non Apice / Pedice

339 surrounding kyanite (Figs. [4 d, e, f](#); [6 b, c](#); [4 d, e, f](#) [7 c](#)) consist of anorthite-rich plagioclase  
340 ( $An_{84}$ ), spinel ( $XMg = 0.558$ ) and minor ~~Al-rich~~peraluminous sapphirine ( $XMg = 0.834$ ; Al  
341 [4.7719](#) a.p.f.u. on the basis of [7-28](#) cations). [An outer corona of orthopyroxene \( \$XMg = 0.70\$ ;](#)  
342 [Table 2\)](#) surrounds sometimes these symplectites (supplementary Fig. SM e, f). Sapphirine in  
343 [these symplectites is very rich in Al \(19.00 a.p.f.u. on the basis of 28 cations\), being](#)  
344 [intermediate between the \(7 : 9 : 3\) and the \(3 : 5 : 1\) end-members.](#)

345

#### 346 *Mafic eclogites (ME)*

347 Compared to ~~the kyanite the~~ eclogites E, mafic eclogites (ME) contain a higher amount of  
348 garnet (Fig. [4 g](#)). Garnet is zoned ([supplementary figure SM4 c, d](#)), displaying [an](#) average  
349 core composition  $Alm_{40}Py_{35}Gr_{24}Sp_1$ , which is only slightly enriched in Fe compared to [garnet](#)  
350 [cores in](#) type E eclogites. However, garnet rims in contact with surrounding plagioclase +  
351 magnesianhornblende symplectites are considerably Fe- and Mn-richer up to  
352  $Alm_{55}Gr_{20}Py_{19}Sp_6$ . Often, garnet porphyroclasts are completely replaced by amph + pl  
353 symplectitic intergrowths. Magnesianhornblende, associated with albite-rich plagioclase, is a  
354 common phase also in symplectites after omphacite. In ME eclogites, cpx + pl symplectites  
355 are rarely preserved. One of these cpx + pl symplectites has been analysed using the same  
356 method described above for eclogites E, yielding the composition  $Di_{58}Jd_{28}Hd_{15}$  for the former  
357 omphacite, showing higher Fe and lower Jd contents compared to eclogites E. Among relict  
358 [eclogite-facies](#) minerals, quartz occurs in mafic eclogites, but its modal abundance is lower  
359 compared to eclogites E. Zoisite, K-feldspar ( $Or_{99}$ ) and pargasitic amphibole ( $XMg = 0.68$ )  
360 occur as  $>100 \mu m$  porphyroclasts (Fig. [6 5e, f](#)). Accessory ~~phases~~ rutile, ilmenite, apatite and  
361 ~~Fe-Cu~~ sulphides are abundant. A single  $30\text{-}\mu m$  crystal of dolomite ( $Ca_{1.00}Mg_{0.88}Fe_{0.12}(CO_3)_2$ )  
362 has been observed included in a garnet core ([supplementary figure SM4 d](#)). ~~Not~~ [Neither](#)  
363 [kyanite](#) ~~neither nor~~ symplectites after kyanite were observed in mafic eclogites.

364

#### 365 *High-Al eclogites (HAE)*

366 These rocks contain no or very minor garnet. Porphyroclastic kyanite, quartz, emerald-  
367 green Fe- and Cr-bearing zoisite (up to 2 cm in size, Fig. [3f](#); 0.95 wt% FeO and 0.24 wt%  
368  $Cr_2O_3$ ) are accessory minerals. Zoisite contains minor inclusions of pargasite, [and is](#)  
369 [commonly replaced by symplectites consisting of almost pure anorthite \( \$An\_{99}\$ \) \(Fig. \[4 h\]\(#\)\).](#)

370 The rock matrix is mainly constituted by [symplectites made of ~~epx+pl~~low-Jd](#)  
371 [clinopyroxene, high-Ab plagioclase and magnesianhornblende. ~~and pl+sp+sapp+cor~~](#)  
372 [symplectites in equal amounts \(Fig. \[5\]\(#\)\).](#) On the basis of the modal abundance of cpx and pl in

Formattato: Tipo di carattere:  
Corsivo

Formattato: Pedice

Formattato: Rientro: Prima riga:  
0,5 cm

373 symplectites after omphacite, the composition of the latter has been reconstructed as  
374  $\text{Di}_{59}\text{Jd}_{33}\text{Hd}_8$ , which is nearly identical to that of omphacite observed in eclogites E. Similarly  
375 to eclogites E, symplectites after kyanite contain anorthite-rich plagioclase ( $\text{An}_{87g}$ ), spinel  
376 ( $\text{XMg} = 0.5964$ ) and Al-rich sapphirine ( $\text{XMg} = 0.857$ ; Al 4.89 19.50 a.p.f.u. on the basis of  
377 728 cations), similarly to eclogites E. Symplectites after kyanite contain anorthite-rich  
378 plagioclase ( $\text{An}_{88}$ ), spinel ( $\text{XMg} = 0.61$ ) and Al-rich sapphirine ( $\text{XMg} = 0.87$ ; Al 4.89 a.p.f.u.  
379 on the basis of 7 cations), similarly to eclogites E. However, in HAE eclogites these  
380 symplectites often contain also corundum (Fig. 7 d, e) (Fig. 5h). Late margarite and  
381 laumontite are also commonly observed as alteration products of these symplectites.  
382 Corundum has been found also in symplectites surrounding zoisite (Fig. h), associated to  
383 anorthite-rich plagioclase ( $\text{An}_{93}$ ), spinel and sapphirine (Fig. 5g).

384  
385  
386 *Amphibole-plagioclase gneisses (AG) - retrogressed eclogites*

387 These rocks display a broadly layered microtexture both at the meso- and microscale,  
388 with mm-sized layers rich in plagioclase and layers rich in amphibole. Plagioclase is typically  
389 Ca-rich ( $\text{An}_{90}$ ), comparable to plagioclase found in coronas surrounding zoisite (cf. eclogites  
390 HAE) and in symplectites replacing kyanite (cf. eclogites E and HAE). However, neither  
391 spinel nor sapphirine nor corundum were observed in these plagioclase layers. Amphibole is  
392 magnesiohornblende ( $\text{XMg} = 0.82$ ), partially replaced by tremolite. Phlogopite also occurs,  
393 partially replaced by chlorite. Occasionally, relict cpx + pl symplectites after omphacite can  
394 be observed. The reconstructed composition of the former omphacite is  $\text{Di}_{67}\text{Jd}_{24}\text{Hd}_9$ ,  
395 displaying lower jadeite content with respect to the more preserved eclogites described above.

## 397 **PETROLOGY AND GEOTHERMOBAROMETRY OF DURIA ROCKS**

398 In the previous sections, we characterized different types of rocks from the Duria area  
399 displaying relict eclogite-facies minerals, namely garnet in peridotites, and omphacite, garnet,  
400 and kyanite and zoisite in eclogites, partially replaced by symplectitic intergrowths containing  
401 at times srilankite and sapphirine in peridotites, and sapphirine, spinel and corundum in  
402 eclogites. In detail, we focused on i) garnet bearing peridotites from Monte Duria and Borgo,  
403 and ii) eclogites, from the Borgo outcrop only. In order to constrain the petrological processes  
404 occurred in these rocks and the  $P$ ,  $T$  conditions in force during eclogite-facies and post-  
405 eclogitic metamorphism, we performed classical thermobarometry and thermodynamic  
406 modelling of both peridotites and mafic rocks.

Formattato: Rientro: Prima riga:  
0,5 cm

Formattato: Tipo di carattere:  
Corsivo

Formattato: Tipo di carattere:  
Corsivo

407

## 408 Garnet peridotites

### 409 Thermobarometry

410 P, T, Temperature conditions of the eclogite facies and post-eclogite metamorphism have  
411 been estimated in peridotites using i) the cpx-opx pyroxene solvus thermometers of (Brey and  
412 Koehler, 1990) and (Taylor, (1998) (TaOpx/Cpx; red in Fig. 8); ii); and the Ca-in-opx  
413 thermometer of Brey & Köhler (1990) corrected by (Nimis and Grütter, (2010)  
414 (BKOpx\_corrNG; purple in Fig. 8); iii) the thermometer of Nimis and Grütter (2010), based  
415 on the Fe-Mg exchange between opx and gt (NGOpx/Gt; black in Fig. 8) and iv) the single  
416 cpx thermometer of (Nimis & Taylor, (2000), based on the enstatite content of cpx  
417 (NTCpx; pink in Fig. 8).

418 Minimum pPressure estimates of the eclogite facies were retrieved using i) the barometer  
419 of (O'Neill, (1981) ( $P_{\text{ONS}+}$ ), based on the transition between spinel lherzolite and  
420 garnet+spinel lherzolite, which is dependent on the Cr/Al+Cr ratio of spinel (O'NSp/Gt; blue  
421 in Fig. 8); ii) the barometer of Taylor (1998), based on the Al exchange between opx and gt  
422 (TaOpx/Gt; grey in Fig. 8); iii) the Cr-in-Cpx barometer of (Nimis & Taylor, (2000),  
423 based on the Cr exchange between cpx and gt (NTCrCpx; green in Fig. 8). Because  
424 O'NSp/Gt  $P_{\text{ONS}+}$  estimates were retrieved using the most Cr-rich composition of relict spinel  
425 included in garnet or in the matrix, they should be considered as minimum estimates.

426 Other estimates of the eclogite peak were retrieved using also the thermometer of (Nimis  
427 and Grütter, 2010), based on the Fe-Mg exchange between opx and gt, and the barometer of  
428 Taylor (1998), based on the Al exchange between opx and gt.

429 The minerals inEstimates for the Duria peridotite sample A2C2 have been retrieved by  
430 considering the core compositions of porphyroblastic garnet, of orthopyroxene and spinel in  
431 the matrix, and of clinopyroxene included in garnet (Table 2). Minerals display a good degree  
432 of equilibration, as the seven independent geothermobarometers yield concordant values and  
433 intersect one to another at  $2.8 \pm 0.2$  GPa and  $730 \pm 20$  °C (Fig. 8). In the other peridotites  
434 from Mt. Duria (MD20, MD25) and Borgo (B1, B3), are not in equilibrium with respect to all  
435 elements, resulting in Fe-Mg and pyroxene-solvus temperatures are often discordant,  
436 suggesting disequilibrium among the considered phases (Fig. 7). In particular, although the  
437 TaOpx/Cpx and the NTCpx thermometers are broadly comparable to sample A2C2,  
438 intersecting the barometers at 700–760°C (with the remarkable exception of sample B3 at  $T =$   
439 830–840°C), the BKOpx\_corrNG thermometer yields generally lower temperatures, down to  
440 680°C in sample MD20. On the contrary, the NGOpx/Gt appears to be shifted at higher

Formattato: Tipo di carattere: Non Corsivo

Formattato: Tipo di carattere: Non Corsivo

Formattato: Tipo di carattere: Corsivo

441 temperatures, intersecting the O'NSp/Gt barometer at 2.8 GPa and 880°C in sample B1 and at  
442 3 GPa and 920°C in sample B3. Excluding sample A2C2, in all other samples the NGOpx/Gt  
443 thermometer displays a second intersection point with both the barometers TaOpx/Gt and  
444 NTCrCpx at anomalously high  $P$ - $T$  conditions, up to around 4 GPa and 1100°C in sample B3  
445 (Fig. 8). The apparently highest temperatures for the eclogite facies stage are those based on  
446 the pyroxene solvus thermometers in sample A2C2 from Monte Duria ( $T = 869^\circ\text{C}$  at  $P_{\text{O'NSp}} =$   
447 2.69 GPa) and those based on the Fe-Mg exchange between opx and gt in sample B1 from  
448 Borgo ( $T = 903^\circ\text{C}$  at  $P_{\text{O'NSp}} = 2.87$  GPa). In sample B3 from Borgo, the thermometers of Brey  
449 & Köhler (1990) and (Nimis and Grütter, 2010) yields concordant  $T = 860 \pm 2^\circ\text{C}$  at  $P_{\text{O'NSp}} =$   
450 2.86 GPa. ~~Because  $P_{\text{O'NSp}}$  estimates were retrieved using the most Cr-rich composition of~~  
451 ~~relict spinel included in garnet or in the matrix, they should be considered as minimum~~  
452 ~~estimates.~~

Formattato: Tipo di carattere:  
Corsivo

Formattato: Tipo di carattere:  
Corsivo

453 Temperature for the post eclogitic peak were estimated by using the thermometers  
454 TaOpx/Cpx, BKOp<sub>x</sub> corrNG, NTCpx and the experimentally calibrated thermometer of Sato  
455 *et al.* (2006), based on the Fe-Mg exchange between spinel and sapphirine (SSp/Sapp; brown  
456 in Fig. 9). Maximum pressure estimates were retrieved by using the barometer O'NSp/Gt,  
457 which represent the upper boundary of the garnet-free field in the presence of low Cr/Al+Cr  
458 keyphitic spinel. The composition of minerals forming kelyphites replacing garnet and opx  
459 coronas replacing olivine was considered for the calculations.

460 Mineral compositions in symplectites kelyphites post-dating eclogite-facies metamorphism  
461 result in discordant temperature estimates, suggesting also in this case a high degree of  
462 disequilibrium. The highest apparent temperatures of  $T = 880^\circ\text{C}$  at  $P_{\text{max}} = 1.6\text{--}1.7$  GPa, based  
463 ~~on~~ retrieved using the the SSp/Sapp thermometer pyroxene solvus thermometers, has have  
464 been observed in Monte Duria peridotites MD20 and MD25 (Fig. 9) ( $T = 858^\circ\text{C}$  at  $P_{\text{O'NSp}} =$   
465 1.58 GPa). Similar temperatures have been calculated for sample A2C2 using the pyroxene-  
466 solvus thermometers TaOpx/Cpx and NTCpx, which yield concordant temperatures of 840°C  
467 at  $P_{\text{max}} = 1.4$  GPa. However, in the same sample the thermometer BKOp<sub>x</sub> corrNG provides  
468 lower temperatures of 635°C at  $P_{\text{max}} = 1.4$  GPa. Pyroxene-solvus temperatures are low and  
469 often discordant also in the other peridotites. Given the partial low-P (LP), high-T (HT) re-  
470 equilibration, suggesting that these temperatures merely represent minimum estimates of the  
471 LP-post-eclogitic peak temperature, e, while  $P_{\text{O'NSp}}$  estimates should be considered as  
472 maximum estimates of the LP-HT sp bearing, gt free metamorphic stage.

Formattato: Tipo di carattere:  
Corsivo

Formattato: Tipo di carattere:  
Corsivo

Formattato: Tipo di carattere: Non  
Corsivo

Formattato: Tipo di carattere:  
Corsivo

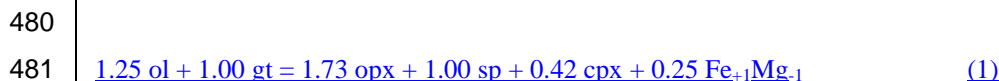
Formattato: Pedice

Formattato: Tipo di carattere: Non  
Corsivo

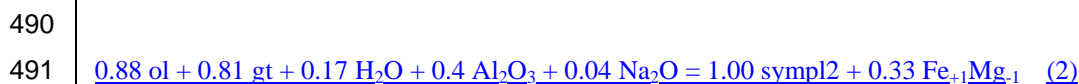
473  
474

475 *Thermodynamic modelling of sapphirine-bearing symplectites*

476 In all Duria peridotites we observed kelyphites developing at the contact between olivine and  
477 garnet consisting of orthopyroxene, spinel and clinopyroxene. By mass-balancing the mineral  
478 compositions of sample MD20 (symp11 in Table 2), we obtained the following reaction  
479 accounting for the formation of these kelyphites:



482  
483 However, in the same sample we observed also kelyphites containing sapphirine associated  
484 with low-Cr spinel, Al-rich orthopyroxene and magnesiohornblende, developed along garnet  
485 fractures. The chemical bulk composition of the symplectite (MD\_20 X1 in supplementary  
486 Table SM2) has been retrieved using the kelyphite mineral compositions (symp12 in Table 2)  
487 and the phase proportions obtained by image analysis of elemental X-ray maps  
488 (supplementary Fig. SM7). The reaction accounting for the formation of sapp-bearing  
489 kelyphites is:



492  
493 where symp12 is the reconstructed bulk composition of the sapph-bearing kelyphite  
494 normalized to 10 cations, and  $\text{Fe}_{+1}\text{Mg}_{-1}$  represents a vector accounting for the Fe–Mg  
495 exchange between reactants and products. Reaction (2) suggests that the growth of sapp-  
496 bearing kelyphites requires higher gt/ol ratios compared to reaction (1), the presence of water  
497 and the addition of Na and extra Al in the system.

498 The  $P$ – $T$  pseudosection calculated for symp12 composition in the system NCFMASH at  
499 water-saturated conditions shows that sapphirine is stable only at relatively low pressure,  
500 below 1.0–1.1 GPa for temperatures ranging from 800 °C to 1000°C (Fig. 10 a). Sapphirine  
501 associated with orthopyroxene, spinel and amphibole is restricted to a narrow field extending  
502 from 0.8 to 1.0 GPa and  $T > 720^\circ\text{C}$ . The intersection of this field and the thermometer  
503 SSp/Sapp occurs at  $P = 0.8$ – $0.9$  GPa and  $T \approx 850^\circ\text{C}$ .

504 A  $T$ – $X$  binary phase diagram has been calculated at fixed  $P = 0.9$  GPa (Fig. 10 b), where  $X =$   
505 0 represents the composition of opx + cpx + sp kelyphites (symp11 in Table 2), derived from  
506 reaction (1), and  $X = 1$  represents the bulk composition symp12 (Fig. 10 b). Sapphirine is  
507 never stable for bulk compositions towards  $X = 0$ , where the assemblage opx + cpx + sp is  
508 stable for  $T > 790^\circ\text{C}$ . For  $X > 0.7$  and  $T > 780^\circ\text{C}$ , sapphirine becomes stable against chlorite +

Formattato: Pedice

Formattato: Tipo di carattere:  
Corsivo

Formattato: Tipo di carattere:  
Corsivo

Formattato: Tipo di carattere:  
Corsivo

Formattato: Tipo di carattere:  
Corsivo

509 [corundum, forming at  \$X = 1\$  the assemblage  \$\text{opx} + \text{sapp} + \text{amph} + \text{sp} + \text{cpx}\$  for  \$T > 820^\circ\text{C}\$ .](#)  
510 [With the exception of clinopyroxene, this last assemblage is consistent with that observed in](#)  
511 [sapp-bearing kelyphites.](#)

Formattato: Tipo di carattere:  
Corsivo

Formattato: Tipo di carattere:  
Corsivo

#### 514 *Thermodynamic modelling of srilankite-bearing symplectites*

515 The occurrence of srilankite ( $\text{Zr}_{0.33}\text{Ti}_{0.66}\text{O}_2$ ) and zircon in a corona replacing garnet and  
516 olivine in sample A2C2 from [Monte-Mt. Duria \(Fig. 5\)](#) gave us the opportunity to perform a  
517 thermodynamic modelling in order to retrieve additional [P, P-T](#) constraints for the post-  
518 eclogitic metamorphic stage.

Formattato: Tipo di carattere:  
Corsivo

Formattato: Tipo di carattere:  
Corsivo

519 Although it is known that the Zr content in rutile is temperature dependent (e.g., ~~Zack~~ *et al.*, 2004), the solid solution between  $\text{TiO}_2$  and  $\text{ZrO}_2$  has been investigated experimentally in  
520 detail only in a few works (McHale & Roth, 1983; ~~TOMKINS~~ *et al.*, 2007; Troitzsch *et al.*,  
521 2004; Troitzsch and Ellis, 2004; [Tomkins \*et al.\*, 2007](#)). In particular, Troitzsch *et al.* (2004)  
522 dealt with the solid solutions among rutile ( $\text{TiO}_2$ ), baddeleyite ( $\text{ZrO}_2$ ) and the intermediate  
523 compound srilankite ( $(\text{Zr,Ti})_2\text{O}_4$ ) at 800–1220°C up to 2 GPa, ~~demonstrating that the~~  
524 ~~composition of ordered srilankite is depending on  $P$  and  $T$ , ranging from  $X_{\text{Ti}}$~~   
525 ~~( $=\text{TiO}_2/(\text{ZrO}_2 + \text{TiO}_2)$ ) 0.60 at 1200°C and 2 GPa, to 0.68 at 800°C and 2 GPa.~~ These  
526 experimental data allowed us to develop a solid solution model and to calculate  $T$ - $X$  and  $P$ - $T$   
527 phase diagrams in petrological systems of increasing complexity (Fig. [810; supplementary](#)  
528 [Fig. SM6](#)). [Details on the solution model can be found as Supplementary information.](#)

530 [The  \$T\$ - \$X\$  phase diagram calculated for the  \$\text{TiO}\_2\$ - \$\text{ZrO}\_2\$  system at 2.0 GPa \(Fig. 8a\)](#)  
531 [reproduces almost perfectly the experimental Ti contents of baddeleyite and the Zr content of](#)  
532 [rutile in function of  \$T\$ . However, the model overestimates the  \$X\_{\text{Ti}}\$  of the intermediate](#)  
533 [compound  \$\(\text{Zr,Ti}\)\_2\text{O}\_4\$  \( \$X\_{\text{Ti}}^{\text{sril}}\$ \) at  \$T > 800^\circ\text{C}\$ . On the basis of the experimental data of](#)  
534 [Troitzsch \*et al.\* \(2004\), the measured composition of srilankite in sample A2C2 \( \$X\_{\text{Ti}} = 0.66\$ \)](#)  
535 [is consistent with  \$T \sim 900^\circ\text{C}\$ , which is close to the temperatures estimated for the post-](#)  
536 [eclogitic peak using the pyroxene solvus thermometers.](#)

Formattato: Evidenziato

537 Because srilankite has been found included in an opx corona replacing olivine (Fig. 5 b),  
538 and associated to opx+cpx+sp in a kelyphite replacing garnet (Fig. 5 d), thermodynamic  
539 modelling has been performed [also in the more complex in the systems  \$\text{MSMgO-SiO}\_2\$ -](#)  
540 [+ \$\text{TiO}\_2\$ - \$\text{ZrO}\_2\$  \(grey chemographies and dashed line in Fig. 11\) and  \$\text{CaO-FeO-MgO-Al}\_2\text{O}\_3\$ -](#)  
541 [+ \$\text{SiO}\_2\$ -FMAS+ \$\text{TiO}\_2\$ - \$\text{ZrO}\_2\$  \(black solid lines in Fig. 11\).](#)

Formattato: Pedice

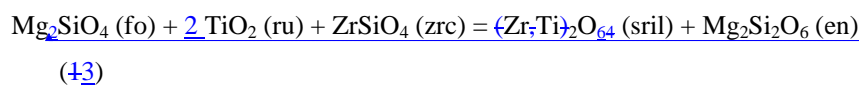
Formattato: Pedice

Formattato: Pedice

Formattato: Pedice

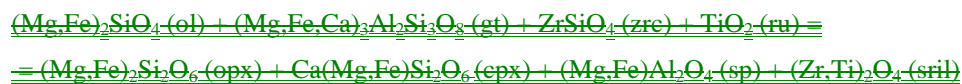


542 In the system  $\text{MgO-SiO}_2\text{-TiO}_2\text{-ZrO}_2\text{-MS+TiO}_2\text{-ZrO}_2$ , chemographies in Figure 8b show  
 543 that the assemblage a peridotitic assemblage forsterite + enstatite should always coexist with  
 544 + zircon + and rutile is stable independently from the bulk composition at relatively low  
 545 temperatures (e.g.,  $T < 830^\circ\text{C}$  at  $P = 0.9\text{ GPa}$ ; Fig. 11).relatively low temperatures.-At higher  
 546 temperatures, the stable assemblage is dependent on the bulk XTi ratio ( $X\text{Ti}^{\text{bulk}} =$   
 547  $\frac{\text{TiO}_2}{(\text{ZrO}_2+\text{TiO}_2)}$ ), becoming either forsterite+enstatite+zircon+srilankite for  $X\text{Ti}^{\text{bulk}} <$   
 548  $X\text{Ti}^{\text{sril}}$  (green star above the sril-en tie line) or forsterite+enstatite+srilankite+rutile for  $X\text{Ti}^{\text{bulk}}$   
 549  $> X\text{Ti}^{\text{sril}}$  (blue star below the sril-en tie line). The reaction leading to the formation of  
 550 srilankite in the  $\text{MgO-SiO}_2\text{-TiO}_2\text{-ZrO}_2$  system therefore is:



555 which is represented with a grey dashed line in the  $P$ - $T$  field shown on a  $P$ - $T$  diagram in  
 556 Figure 8 b (Fig. 11). Our model predicts that the above univariant reaction occurs at  
 557 temperatures of about  $79\text{--}10300^\circ\text{C}$  at  $0.54\text{ GPa}$  and  $900^\circ\text{C}$  at  $1.7\text{ GPa}$  in the  $\text{MS+TiO}_2\text{-ZrO}_2$   
 558 system.

559 A  $P$ - $T$  pseudosection (i.e., isochemical section) has been calculated for the system  $\text{CaO-}$   
 560  $\text{FeO-MgO-Al}_2\text{O}_3\text{-SiO}_2\text{-TiO}_2\text{-ZrO}_2\text{-CFMAS+TiO}_2\text{-ZrO}_2$  in order to check how the stability  
 561 of srilankite is influenced by other components  $\text{CaO}$ ,  $\text{FeO}$  and  $\text{Al}_2\text{O}_3$ . In this system By adding  
 562  $\text{FeO}$ , the srilankite-forming reaction univariant above becomes divariant, because olivine and  
 563 orthopyroxene form solid solutions between their Mg- and Fe-endmembers. By adding also  
 564  $\text{CaO}$  and  $\text{Al}_2\text{O}_3$ , (unbalanced) becomes clinopyroxene and spinel become stable, so that the  
 565 actual phase assemblage of the srilankite-bearing kelyphite observed in sample A2C2 can be  
 566 modelled.



571 (2) Therefore, in order to calculate the pseudosection In order to model the low  $P$ ,  
 572 high  $T$  reaction between garnet and olivine in a Zr- and Ti bearing system, we considered a  
 573 the bulk composition of the kelyphite, retrieved by mass-balancing the compositions of the  
 574 reactant  $\text{gt} + \text{ol}$ , and the kelyphite products  $\text{opx} + \text{cpx} + \text{sp}$  occurring in sample A2C2 (Table  
 575 2), doped with 3 mol% rutile and 1 mol% zircon (Table SM 2), consisting of garnet and

Formattato: Tipo di carattere:  
Corsivo

Formattato: Pedice

Formattato: Pedice

Formattato: Pedice

Formattato: Pedice

Formattato: Tipo di carattere:  
Corsivo

Formattato: Tipo di carattere:  
Corsivo

Formattato: Tipo di carattere:  
Corsivo

Formattato: Tipo di carattere:  
Corsivo

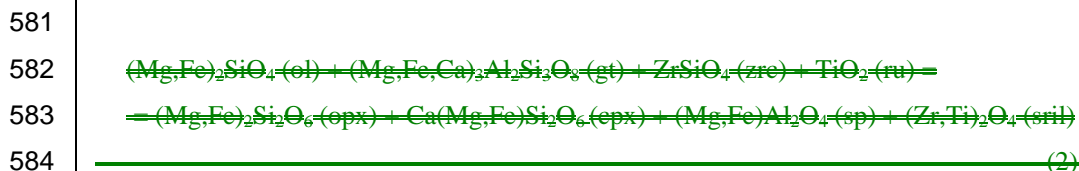
Formattato: Pedice

Formattato: Pedice

Formattato: Pedice

Formattato: Pedice

576 ~~olivine in equal amounts, using the mineral compositions measured in garnet peridotite A2C2,~~  
 577 ~~and~~ assuming a bulk  $X_{Ti} = 0.75$  (Fig. 9c) and  $X_{Ti} = 0.25$  (Fig. 9d). In this more complex  
 578 system, the stability of srilankite is ~~expanded~~ shifted at lower temperatures at lower  
 579 temperatures by around 20°C (Fig. 11) ~~and is not dependent on the bulk  $X_{Ti}$ . In this system,~~  
 580 ~~the srilankite forming reaction (unbalanced) becomes:~~



585 meaning that  
 586 In the pseudosections, srilankite in equilibrium with opx, ± sp and cpx is should be  
 587 formed stable against at the expenses of either zircon ± (Fig. 8c) or rutile (Fig. 8d), depending  
 588 on  $X_{Ti}^{bulk}$ , at  $T, T = \geq 810-970-1000^\circ C$  at 0.9 GPa. This temperature is higher consistent  
 589 with compared to that estimated those retrieved for the post-eclogitic peak by using the  
 590 TaOpx/Cpx and NTCpx thermometers (820–830°C at 0.9 GPa; sample A2C2) and the  
 591 SSp/Sapp thermometer (850°C at 0.9 GPa; samples MD20 and MD25). for the post-eclogitic  
 592 peak using the pyroxene solvus thermometers.

593 However, at this stage the uncertainties associated to the temperatures retrieved from this  
 594 new thermodynamic model are difficult to predict. Looking forward to experimental  
 595 constraints in more complex systems, we can infer that in natural systems the stability field of  
 596 srilankite could be shifted most likely at lower temperatures by 50–100°C.

## 598 Eclogites

### 599 Thermobarometry

600 ~~Temperatures-P-T~~ conditions of the eclogite-facies and of the post-eclogitic peaks have  
 601 been estimated for type "E" eclogites (sample B5), representative of the average mafic rocks  
 602 of Duria.

603 Temperatures for the eclogitic peak have been retrieved by using the thermometer of  
 604 (Krogh-Ravna, (2000), based on the Fe-Mg exchange between cpx and gt (cpx-gt in Fig. 12  
 605 a). Peak pressures were estimated by using the barometer of Ravna and Terry (2004), based  
 606 on the net transfer reaction diopside + kyanite = grossular + pyrope + quartz/coesite (gt-cpx-  
 607 ky-qtz/coe in Fig. 12 a). The composition of preserved omphacite crystals included in kyanite  
 608 and of porphyroclastic garnet cores have been used for the calculations (Table 2). Additional  
 609  $T, T$  estimates have been retrieved using the trace-based thermometers ~~±~~ Zr-in-rutile

Formattato: Tipo di carattere:  
Corsivo

Formattato: Evidenziato

Formattato: Tipo di carattere:  
Corsivo

Formattato: Tipo di carattere:  
Corsivo

Formattato: Tipo di carattere:  
Corsivo

610 ~~calibration after~~ Tomkins et al. (2007) (Zr-in-ru in Fig. 12), ~~calibration after Tomkins et~~  
611 ~~al., 2007~~, considering the Zr content in rutile included in garnet (343–352 ppm Zr; see Table  
612 4).; ii) Ti in quartz (calibration after Wark & Watson, 2006), considering the Ti content of  
613 porphyroclastic quartz. Zr in rutile ranges from 343 to 621 ppm, which corresponds to a T  
614 range from 660°C to 712°C, while the average Ti content in quartz is 43 ppm, corresponding  
615 to T = 654°C (Fig. 9). This temperature range intersects the temperatures estimated using the  
616 cpx-gt thermometer at pressures between 1.5 and 2.5 GPa.

617 The intersection of the thermometers cpx-gt and Zr-in-ru with the barometer gt-cpx-ky-  
618 qtz/coe provides a concordant estimate of peak conditions at  $P = 3.0$  GPa and  $T = 740$ –  
619  $750$ °C, slightly above the quartz/coesite transition (dashed line in Fig. 12 a) These pressures  
620 are higher than those estimated by using the Jd in cpx barometer of Holland (1980) (1.35 GPa  
621 at 700°C), based on the reaction albite = jadeite + quartz and the jadeite content in omphacite,  
622 which provides minimum estimates for omph-bearing assemblages.  $P$

623  $\leq 2.5$  GPa at  $T = 700$ °C are consistent with the presence of pargasitic amphibole in the  
624 eclogite-facies peak assemblage, which should disappear at 2.4 GPa at 700°C for MORB  
625 compositions at H<sub>2</sub>O-saturated conditions (Schmidt and Poli, 1998; Fig. 9). It is noteworthy  
626 that the estimated P, T conditions for the eclogitic peak are close to the experimental wet  
627 solidus of MORB basalts, but dehydration melting temperatures in fluid-absent zoisite-  
628 bearing eclogites are as high as 1000°C at 2.4 GPa (Skjerlie and Patino Douce, 2002).

629 The  $P, T, T$  conditions of the post-eclogitic peak have been estimated using the  
630 compositions of the minerals forming symplectites replacing kyanite, garnet and omphacite,  
631 and those of garnet rims in contact with them. In particular, orthopyroxene found in a relict  
632 opx+pl-symplectite replacing garnet-kyanite in contact with relict garnet (Fig. 7 c;  
633 supplementary Fig. SM7) was considered for the Ca-in-opx thermometer of Brey & Köhler  
634 (1990) corrected by Nimis and Grütter (2010), and for the barometer of Lal (1993), based on  
635 the net transfer reaction reactions enstatite + anorthite = pyrope + grossular + quartz (gt-  
636 opx-pl-q in Fig. 12 b). Clinopyroxene forming cpx+pl symplectites replacing omphacite in  
637 contact with relict garnet was used for the barometer of (Eckert et al., 1991), based on the  
638 reaction net transfer diopside + anorthite = pyrope + grossular + quartz (gt-cpx-pl-q in Fig.  
639 12 b). Temperature for the post eclogitic peak were estimated also by using the thermometer  
640 of (Sato et al., (2006), based on the Fe–Mg exchange between spinel and sapphirine (sapp-sp  
641 in Fig. 12), assemblage found in symplectites replacing kyanite (e.g., Fig. 7 c), and by using  
642 the thermometer Zr-in-ru, considering the Zr content of rutile embedded in symplectites (567–  
643 845 ppm Zr; Table 4).-

Formattato: Tipo di carattere:  
Corsivo

Formattato: Tipo di carattere:  
Corsivo

Formattato: Non Evidenziato

Formattato: Evidenziato

Formattato: Evidenziato

Formattato: Evidenziato

Formattato: Tipo di carattere:  
Corsivo

Formattato: Tipo di carattere:  
Corsivo

644 The highest  $P$ ,  $P$ - $T$  conditions and  $T$ ,  $T = 850$ – $850$  °C at  $P = 1.2$ – $0.8$ – $1.0$  GPa, are  
645 provided by the intersection of the barometers gt-opx-pl-q and gt-cpx-pl-q, barometer and the  
646 thermometer sapp-sp thermometer, while  $T$ ,  $T$  estimated using the Ca-in-opx ( $755$ – $760$  °C at  
647  $0.85$ – $0.95$  GPa) and the Zr-in-ru ( $690$ – $740$  °C at  $0.85$ – $0.95$  GPa) thermometer thermometers is  
648 are slightly considerably lower, suggesting partial re-equilibration during retrogression ( $822$  °C  
649 at  $1.2$  GPa).

650 Peak These  $P$ ,  $T$ ,  $P$ - $T$  conditions retrieved for type "E" eclogites, which are very close to  
651 the experimental gt-in and well above the wet solidus reported by Schmidt & Poli (1998)  
652 (grey dashed lines in Fig. 9), are comparable to  $P$ ,  $T$ ,  $T$  conditions retrieved estimated in  
653 Duria peridotites for both the eclogite-facies ( $P \approx 3.0$  GPa and  $T \approx 750$  °C) and the post-  
654 eclogitic LP-HT metamorphism ( $P \approx 0.9$  GPa and  $T \approx 850$  °C) in peridotites.

#### 655 Thermodynamic modelling

657 The bulk composition of type "E" eclogite B5 was considered for the calculation of  $P$ - $H_2O$   
658 and  $P$ ,  $T$ ,  $P$ - $T$  (Fig. 10a) and  $P$ - $X$  (Fig. 10b, Fig. 11a) pseudosections in the system  
659 KNCFMASH (Fig. 13). The  $P$ - $H_2O$  pseudosection (Fig. 13 a), calculated at fixed  $T = 750$  °C  
660 in the light of  $T$  estimated by means of conventional thermometry, serves to estimate the  
661 amount of the component  $H_2O$  accounting for the presence of K-feldspar in Duria mafic  
662 rocks, occurring as a relict eclogite-facies phase together with garnet, omphacite, kyanite and  
663 quartz. In figure 13 a,  $X$  represents the  $H_2O$  component added to the dry bulk composition B5  
664 (Table 1; see also supplementary Table SM2). K-feldspar is stable with garnet, omphacite,  
665 kyanite quartz and phengite for  $P > 1.8$  GPa and a maximum bulk  $H_2O$  content of 0.1 wt%,  
666 above which K-feldspar disappears. Therefore, a  $H_2O$  undersaturated conditions with bulk  
667  $H_2O$  contents below 1 wt% are needed to stabilise K feldspar at  $P > 1.7$  GPa (Fig. 10b),  
668 observed as porphyroclasts in Borgo eclogites type "E" and "ME". However, at these  
669 pressures bulk  $H_2O$  contents  $> 1$  wt% are necessary for the stability of pargasitic amphibole,  
670 often found in type "E" eclogites.  $P$ ,  $T$ ,  $T$  pseudosection shown in Figure 10a is has been  
671 calculated with assuming an intermediate bulk  $H_2O$  content of = 0.0054 wt% (Fig. 13 a).  
672 Pseudosections indicate that the  $X$ Or of K-feldspar increases as pressure increases, being 0.97  
673 at 2.5 GPa, 0.98 at 2.7 GPa and 0.99 at 3.0 GPa and 750 °C. These values are comparable to  
674 the K-feldspar compositions measured in samples D3 (0.970–0.978; eclogite type E) and D6  
675 (0.986; eclogite type ME), thus confirming high-pressure conditions up to 3 GPa for these  
676 rocks, suggested by conventional thermobarometry.

Formattato: Tipo di carattere:  
Corsivo

Formattato: Tipo di carattere: Non  
Corsivo

Formattato: Tipo di carattere:  
Corsivo

Formattato: Tipo di carattere:  
Corsivo

Formattato: Tipo di carattere:  
Corsivo

Formattato: Tipo di carattere:  
Corsivo

Formattato: Tipo di carattere:  
Corsivo

Formattato: Tipo di carattere:  
Corsivo

Formattato: Tipo di carattere:  
Corsivo

Formattato: Tipo di carattere:  
Corsivo

Formattato: Tipo di carattere:  
Corsivo

Formattato: Tipo di carattere:  
Corsivo

Formattato: Tipo di carattere:  
Corsivo

Formattato: Pedice

Formattato: Tipo di carattere:  
Corsivo

Formattato: Tipo di carattere:  
Corsivo

Formattato: Tipo di carattere:  
Corsivo

Formattato: Tipo di carattere:  
Corsivo

Formattato: Pedice

Formattato: Tipo di carattere:  
Corsivo

Formattato: Pedice

Formattato: Tipo di carattere:  
Corsivo

Formattato: Pedice

Formattato: Tipo di carattere:  
Corsivo

Formattato: Tipo di carattere:  
Corsivo

677 For this relatively low H<sub>2</sub>O content, the amphibole-out is shifted at lower  
678  $P$  compared with the wet amphibole-out found experimentally by Schmidt & Poli (1998)  
679 (black dashed line in Fig. 10a13 b), and the predicted phase assemblage at 2.5 GPa and 700°C  
680 is omphacite (57 vol%), garnet (29 vol%), quartz (6 vol%), kyanite (5 vol%), K feldspar (2  
681 vol%) and phengite (<1 vol%). At  $T = 750^{\circ}\text{C}$ , amphibole (pargasite) is predicted to be stable  
682 only at  $P < 1.75$  GPa in equilibrium with Na-rich plagioclase, so it is not thought to be a peak  
683 high-pressure phase. Amphibole + K feldspar assemblage is stable at  $P < 1.7$  GPa and  $T =$   
684 700°C independently from the bulk H<sub>2</sub>O content. However, at these  $P, T$  conditions the  
685 predicted composition of K feldspar is relatively Ab-rich and Or-poor (Or<sub>75</sub> at 1.65 GPa and  
686 700°C). K feldspar compositions  $X_{\text{Or}} = 0.970-0.978$ , measured in type "E" eclogites, are  
687 stable at  $P = 2.4-2.6$  GPa at 700°C (fig. 10 a, b), which are comparable to  $P, T$  conditions  
688 estimated for the eclogitic peak through conventional thermobarometry.

Formattato: Pedice

Formattato: Tipo di carattere:  
Corsivo

Formattato: Tipo di carattere:  
Corsivo

Formattato: Tipo di carattere:  
Corsivo

Formattato: Tipo di carattere:  
Corsivo

689 In the  $P, T$  pseudosection, orthopyroxene and spinel, found in symplectites replacing  
690 garnet and kyanite and garnet, respectively, are stable at  $P < 0.9-1.0$  GPa at 850°C (Fig. 13  
691 b). However, symplectites after kyanite contain also sapphirine + spinel, which are never  
692 stable for the composition B5. Bearing in mind that aluminium is a relatively inert  
693 component, we modelled coronitic reactions involving kyanite by calculating a  $P-T-X$   
694 pseudosection at fixed  $P = 0.9$  GPa in the system KNCFMAS, where the sliding composition  
695  $X$  represents a decreasing amount of kyanite component added to the a bulk rock symplectite  
696 composition B5 from 2530 wt% ( $X = 0$  in Fig. 14 4a) to 0 wt% ( $X = 1$  in Fig. 14 4a) (see  
697 supplementary Table SM2). The symplectite compositions has been retrieved by considering  
698 the phase proportions in the micro-domain, obtained by means of image analysis of X-ray  
699 maps, and the phase compositions (sample B5 - Symp2 in Table 2). The retrieved phase  
700 proportions in this micro-domain, excluding the non-symplectitic phases garnet, quartz,  
701 amphibole and rutile, is: Ab-rich plagioclase 37 vol%; clinopyroxene 25 vol%; An-rich  
702 plagioclase 21 vol%; spinel 10 vol%; orthopyroxene 5 vol%; sapphirine 1.5 vol%. In this  
703 way, we modelled the phase stability fields for micro-domains close to kyanite porphyroclasts  
704 interacting with the surrounding rock assuming perfectly dry conditions. The  $T-P-X$   
705 pseudosection calculated at 850°C, assuming a low bulk H<sub>2</sub>O content of 0.01 wt%, shows that  
706 for kyanite-enriched compositions sapphirine

Formattato: Tipo di carattere:  
Corsivo

Formattato: Tipo di carattere:  
Corsivo

Formattato: Tipo di carattere:  
Corsivo

Formattato: Tipo di carattere:  
Corsivo

Formattato: Tipo di carattere:  
Corsivo

Formattato: Tipo di carattere:  
Corsivo

Formattato: Tipo di carattere:  
Corsivo

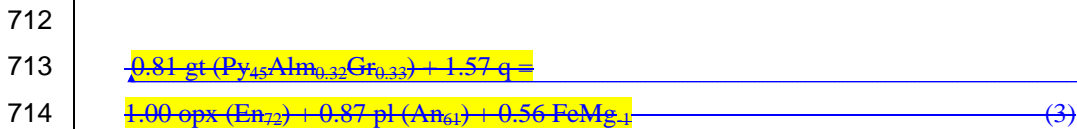
Formattato: Tipo di carattere:  
Corsivo

Formattato: Tipo di carattere:  
Corsivo

Formattato: Tipo di carattere:  
Corsivo

707 the orthopyroxene stability field is expanded at higher pressures, up to 1.25 GPa, which is  
708 nearly coincident with the  $P, T$  estimated using conventional thermobarometry. By balancing  
709 the phase compositions predicted by the thermodynamic model at 2.5 GPa and 700°C

710 (~~reagents~~), and at 1.2 GPa, 850°C and  $X=0.33$  (~~products~~), we obtained the following ~~opx-~~  
711 ~~producing reaction:~~



Formattato: Evidenziato

716 where  $\text{FeMg}_{-1}$  represents a vector accounting for the Fe-Mg exchange between gt and opx.

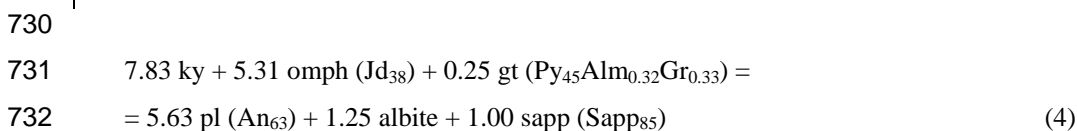
717 The P-X pseudosection shows also that sapphirine-bearing assemblages become stable at  $P$ ,  
718  $P < 0.88$  GPa for bulk compositions enriched in ky (> 23 wt%;  $X < 0.25$  in figure 11 a), but at  
719 these conditions sapphirine coexists with cordierite, which has never been observed in

Formattato: Tipo di carattere:  
Corsivo

720 symplectites. The stability field of sapphirine is expanded up to  $P$ ,  $P = 0.91$  GPa if  $\sim 20$  wt%

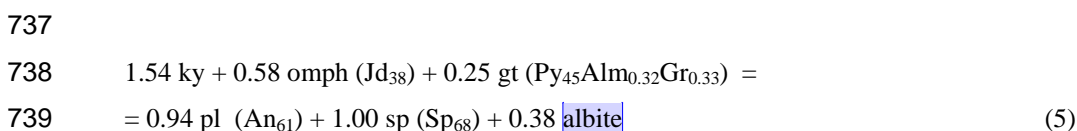
Formattato: Tipo di carattere:  
Corsivo

721 kyanite is added to the bulk rock B5 ( $X = 0.33$  in figure 11 a). At these P, T, X conditions,  
722 sapphirine is in equilibrium with opx, gt, amph and pl. By decreasing the ky content towards  
723 the composition B5, the adjacent fields contain also spinel. This suggests that a small  
724 fluctuation in the kyanite/bulk rock ratio in the micro-domain surrounding a kyanite  
725 porphyroclast that is getting destabilised during LP-HT metamorphism can lead to the  
726 assemblage plagioclase + sapphirine towards the inner part of the reaction front and  
727 plagioclase + spinel towards the outer part of the reaction front. By balancing the phase  
728 compositions predicted by the model at 2.5 GPa and 700°C (~~reagents~~~~reactants~~), and at 0.90  
729 GPa, 850°C and  $X=0.33$  (products), we obtained the following sapp-producing reaction:



734 (cf. Carswell ~~at et~~ al., 1989)

735 and, using the sp and pl compositions predicted at 0.88 GPa, 850°C and  $X=0.4$ , the  
736 following sp-bearing reaction:



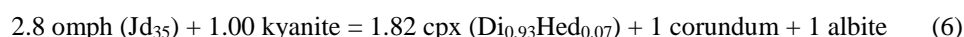
Commento [OU1]: wo  
plagioclases: this is typical of a  
"mosaic" equilibrium, with An at  
the place of kyanite (and zoisite?)  
and An59 after omphacite.

741 Corundum has been found in symplectites replacing kyanite in eclogites type "HAE",  
742 associated to sapphirine, spinel and An-rich plagioclase. In order to constrain the stability

743 field of this assemblage, we performed also for these rocks a P-X pseudosection at fixed  $T$ ,  $T$

Formattato: Tipo di carattere:  
Corsivo

744 = 850°C, where X = 1 accounts for the bulk composition of sample D9 + 0.01 wt% H<sub>2</sub>O, and  
745 X = 0 represents bulk D9 with 30 wt% added kyanite (Fig. 11b). At these conditions,  
746 corundum is stable with sapphirine at P = 1.28 GPa for the composition D9 (X = 1). By  
747 increasing the kyanite/rock ratio, the assemblage corundum + sapphirine becomes stable at  
748 lower P, down to 1.03 GPa at X = 0. Considering the omphacite composition predicted at 2.5  
749 GPa and 700°C, a possible corundum-forming reaction could be:



(Johansson and Möller, 1986).

754 The P-X pseudosection of Figure 11b shows that spinel never coexists with corundum +  
755 sapphirine. Spinel occurs with sapphirine at P < 0.87 GPa and X > 0.3, corresponding to  
756 < 20 wt% of kyanite added to the bulk rock D9, or at P up to 1.23 for composition D9  
757 without addition of kyanite.

758 **Togliere il discorso zoisite** A double corona replacing cm-sized zoisite has been found in  
759 the HAE eclogite D1 (Fig. 5g). The inner corona consists of An-rich plagioclase, while the  
760 outer part is formed by a symplectitic intergrowth of pl+sapp+sp+cor. Because this  
761 symplectite is almost identical to symplectites surrounding kyanite, we developed a model in  
762 order to investigate whether this assemblage can develop also by LP-HT reactions involving  
763 zoisite. Analogously to P-X pseudosections calculated at 850 °C for samples B5 and D9, we  
764 considered a sliding composition from bulk rock D1 + 0.01 wt% of H<sub>2</sub>O (X = 1 in figure 12a)  
765 to D1 enriched with 100 wt% of zoisite (X = 0). Furthermore, we calculated also a X-aH<sub>2</sub>O  
766 pseudosection at fixed P = 1.2 GPa and T = 850°C (Fig. 12b) in order to investigate the  
767 role of H<sub>2</sub>O. The P-X pseudosection shows that zoisite is stable down to P = 1.0 GPa for X  
768 < 0.55, corresponding to 45 wt% of added zoisite. By decreasing the amount of added zoisite,  
769 the stability field of zoisite is shifted at higher pressures. At P = 1.2 GPa, zoisite disappears  
770 at X > 0.55, where the stable assemblage is amph+pl+cpx+H<sub>2</sub>O. At X > 0.9, sapphirine  
771 becomes a stable phase. For compositions close to D1, the assemblage corundum + sapphirine  
772 is stable slightly above 1.2 GPa while spinel + sapphirine are stable slightly below. However,  
773 X-aH<sub>2</sub>O pseudosection calculated at 1.2 GPa and 850°C shows that LP-HT assemblages after  
774 zoisite are highly dependent on water activity (i.e., on the H<sub>2</sub>O chemical potential). For aH<sub>2</sub>O  
775 < -1.50, the breakdown of zoisite will produce An-rich plagioclase only up to X = 0.45 (added  
776 zoisite 54 wt%), which is accomplished by the following reaction:

Formattato: Tipo di carattere:  
Corsivo

Formattato: Tipo di carattere:  
Corsivo

Formattato: Tipo di carattere:  
Corsivo

Formattato: Evidenziato

Formattato: Tipo di carattere:  
Corsivo, Evidenziato

Formattato: Evidenziato

Formattato: Tipo di carattere:  
Corsivo, Evidenziato

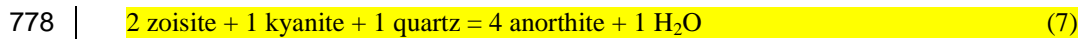
Formattato: Evidenziato

Formattato: Tipo di carattere:  
Corsivo, Evidenziato

Formattato: Evidenziato

Formattato: Tipo di carattere:  
Corsivo, Evidenziato

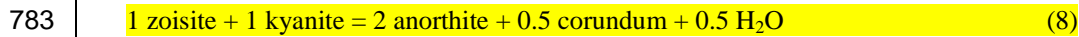
Formattato: Evidenziato



779

780 By decreasing the zoisite content towards composition D1, corundum + plagioclase are  
781 stabilized first, suggesting the following reaction:

782

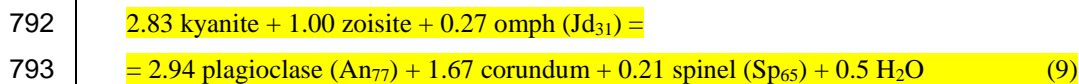


784

785 (cf. O'Brien et al, 1992)

786 A further decrease in added zoisite results in the assemblages spinel + corundum +  
787 plagioclase, spinel + plagioclase, sapphirine + spinel + plagioclase and eventually sapphirine  
788 + plagioclase for the composition D1. The following reactions can be retrieved by considering  
789 as reactants the omphacite predicted at 2.5 GPa and 700°C, and as products spinel, sapphirine  
790 and plagioclase predicted at 1.2 GPa and 850°C.

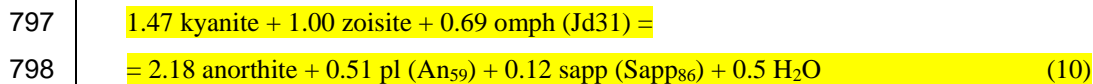
791



794

795 and

796



799

800 Pseudosections suggest that in eclogites HAE the breakdown of both kyanite and zoisite  
801 can end up with anorthite-rich plagioclase associated to spinel, sapphirine and corundum at  
802 1.2 GPa and 850°C, for low H<sub>2</sub>O activities and a proper degree of interaction between  
803 kyanite/zoisite and the other surrounding high-pressure phases, in particular omphacite and  
804 garnet.

805

## 806 DISCUSSION

807

808 It is noteworthy that the estimated P, T conditions for the eclogitic peak are slightly above  
809 the experimental wet solidus of MOR compositions at H<sub>2</sub>O-saturated conditions (Schmidt  
810 and Poli, 1998), but dehydration melting temperatures in fluid-absent zoisite-bearing eclogites  
811 are as high as ≈1000°C at 2.4 GPa (Skjerlie and Patino Douce, 2002).



812

813 In the Duria area, relict eclogite-facies assemblages are still preserved both in garnet-  
814 bearing peridotites and in different types of eclogites. In these rocks, high-pressure phases are  
815 partially or completely replaced by low-P/high-T symplectitic intergrowths (Fig. 4 and 5).

816 Thermodynamic models and thermobarometric data estimated for the Duria garnet  
817 peridotites are consistent with an equilibration at ~~90-100 km~~XX GPa depth and temperatures  
818 of 850-900°C. ~~In garnet peridotites, LP-HT~~R Reactions between garnet and olivine produced  
819 opx coronas on the olivine side, and opx+cpx+sp symplectites on the garnet side. Srilankite  
820 and zircon have been observed in textural equilibrium with these LP-HT minerals (Fig. 5a).  
821 Srilankite is a very uncommon phase in peridotites, and its presence suggests that a certain  
822 degree of metasomatism by a crust-derived Zr-bearing agent, has occurred during the post-  
823 eclogitic stage. Magmatic srilankite has been reported in gabbroic veins cutting oceanic  
824 peridotite in the Southwest Indian Ridge (Morishita *et al.*, 2004), and srilankite inclusions in  
825 upper-mantle pyrope-rich garnet equilibrated at 1.5-3.0 GPa and 600-800 °C have been found  
826 in xenoliths from the Navajo Volcanic Field on the Colorado Plateau (Wang *et al.*, 1999).  
827 Srilankite formed through reaction between ilmenite and baddeleyite has been reported also in  
828 mafic granulites from the Bergen Arcs in Western Norway equilibrated at ~~P,~~P < 1 GPa and  
829 800-850°C (Bingen *et al.*, 2001). At Duria, srilankite composition  $Zr_{0.33}Ti_{0.66}O_2$  suggests  
830 temperatures of equilibration of 850-900°C, which is consistent with temperatures estimated  
831 by Ca-in-opx and opx-gt thermometry. Coherently with the absence of garnet in LP-HT  
832 symplectites and the low Cr-content of symplectitic spinel, conventional barometry suggests  
833 that post-eclogitic ~~metamorphism~~metamorphism of garnet peridotites occurred below ~~~50~~  
834 50-km depth. Chlorite, anthophyllite, phlogopite and magnesiohornblende represent late-  
835 stage, amphibolite-facies intergrowths overprinting high-temperature symplectites.

836 Eclogites from Duria are characterised by a broad major-element N-MORB signature.  
837 Kyanite eclogites (KE), mafic eclogites (ME) and high-Al eclogites (HAE) have been  
838 distinguished on the basis of the bulk chemistry using principal component analysis (Fig. 6).  
839 Magnesiohornblende+plagioclase gneisses (AG) are interpreted as rocks recrystallised in  
840 fluid-rich domains under amphibolite-facies conditions after the high-temperature event ~~and~~  
841 ~~showing ductile flow deformation,~~ and ~~they~~ have not been investigated in detail in this study.  
842 Thermodynamic models and conventional thermobarometric data suggest that kyanite  
843 eclogites from Duria underwent a high-pressure peak at ~80 km depth at temperature of about  
844 700°C. The occurrence of K-feldspar as a high-pressure phase associated with pargasitic  
845 amphibole and zoisite indicates water undersaturated conditions during the eclogitic peak;

Formattato: Tipo di carattere:  
Corsivo

846 ~~therefore characterised by a very low amount of the component H<sub>2</sub>O~~ (Fig. 10b). In eclogites,  
847 the following LP-HT symplectitic intergrowths have been observed: i) opx + pl replacing  
848 garnet; ii) Di-rich, Jd-poor cpx + Ab-rich pl replacing omphacite; iii) An-rich pl ± sp ± sapp ±  
849 cor replacing kyanite and zoisite. Conventional thermobarometry suggests that post-eclogitic  
850 assemblages should have equilibrated ~~below~~ above ~40 km depth at temperatures of about  
851 850°C.

852 ~~However, calculated P-T pseudosections (i.e. isochemical phase diagrams) fail to~~  
853 ~~reproduce~~ The mineral assemblages (iii) observed in symplectites could only be stabilised in  
854 Al<sub>2</sub>O<sub>3</sub>-rich compositional microdomains derived from destabilisation of kyanite. ~~In~~  
855 ~~particular, sapphirine-bearing assemblages are never stable if the bulk composition of kyanite~~  
856 ~~eclogites (E) is considered. We approached this issue by performing a material transfer study,~~  
857 ~~assuming that Al<sub>2</sub>O<sub>3</sub> did not behave as a perfectly mobile component and, consequently, that~~  
858 ~~the composition of the micro-domain surrounding a high-pressure Al<sub>2</sub>O<sub>3</sub>-rich phase replaced~~  
859 ~~by LP-HT minerals (i.e., kyanite and zoisite) is not equivalent to the composition of the bulk~~  
860 ~~rock.~~ Because of the "inert" character of the component Al<sub>2</sub>O<sub>3</sub> (cf. (Korzhinskii, 1959), we  
861 preferred to express the variable content of Al<sub>2</sub>O<sub>3</sub> as an extensive variable (weight amount of  
862 the component Al<sub>2</sub>SiO<sub>5</sub> (kyanite) or Ca<sub>2</sub>Al<sub>3</sub>Si<sub>3</sub>O<sub>12</sub>(OH) (zoisite) added to the bulk-rock  
863 composition), rather than an intensive variable (e.g.,  $\mu\text{Al}_2\text{O}_3$ ) (see also (Tumiati *et al.*, 2015)).  
864 In the phase diagrams performed in order to model the LP-HT symplectites replacing kyanite  
865 (Fig. 11a,b), X represents a sliding bulk composition where X=1 stands for the real bulk-rock  
866 compositions B5 (kyanite eclogite; Fig. 11a) and D9 (high-Al eclogite; Fig. 11b) reported in  
867 Table 1, and X=0 stands for 70 wt% of the same bulk compositions and 30 wt% of added  
868 kyanite component. ~~Phase diagrams demonstrate that sapphirine becomes stable in kyanite-~~  
869 ~~eclogites only for a relatively high added kyanite component (X < 0.4) (Fig. 13) and,~~  
870 ~~therefore, this mineral should form in those areas of the symplectite micro-domain where the~~  
871 ~~component Al<sub>2</sub>SiO<sub>5</sub> poorly re-equilibrated with the surrounding rock. The material transfer~~  
872 ~~study performed through thermodynamic modelling is the best way to model the mineral~~  
873 ~~distribution observed in symplectites.~~

874 Far from these domains, sapphirine-free, spinel+plagioclase symplectites ~~should~~ would  
875 occur. Thermodynamic modelling also ~~shows~~ predicts that ~~considering the kyanite eclogite~~  
876 ~~composition, corundum is~~ should never be stable in LP-HT symplectites replacing kyanite,  
877 consistent with the absence of. ~~In fact, corundum has never been observed~~ in this eclogite  
878 type.

Formattato: Tipo di carattere:  
(Predefinito) Times New Roman,  
12 pt

Formattato: Tipo di carattere:  
(Predefinito) Times New Roman,  
12 pt, Pedice

Formattato: Tipo di carattere:  
(Predefinito) Times New Roman,  
12 pt

Formattato: Tipo di carattere:  
(Predefinito) Times New Roman,  
12 pt, Pedice

Formattato: Tipo di carattere:  
(Predefinito) Times New Roman,  
12 pt

879 ~~Accordingly to petrographic observations, corundum is instead predicted to may~~ form in  
880 high-Al eclogites. ~~This is again consistent with petrographic evidence. since corundum occurs~~  
881 ~~The material transfer study performed through thermodynamic modelling is the best way to~~  
882 ~~model the mineral distribution observed in symplectites, where corundum occurs~~ in the inner  
883 part of the symplectitic pseudomorph after kyanite ( $X < 0.2$ ), and it disappears in the outer  
884 part of the symplectites, where sapphirine and eventually spinel form (Fig. 13).

Formattato: Tipo di carattere:  
(Predefinito) Times New Roman,  
12 pt

### 886 Duria in the Alpine framework

887 The estimated ~~P, T~~ conditions of Duria rocks, ~~850°C and 1.0 GPa~~, point to a ~~granulite~~  
888 ~~granulite-facies~~ metamorphic stage, shared by both peridotites and mafic rocks, postdating a  
889 former eclogite-facies peak ~~at 700-750°C and 2.5-3.0 GPa~~. Granulite-facies assemblages are  
890 in turn overprinted by late ~~Barrovian~~ amphibolite-facies metamorphism. Previous P-T  
891 estimates for the high-pressure metamorphism ~~displayed-evidenced in~~ by garnet peridotite  
892 from Duria ( $3.0 \pm 0.2$  GPa and  $829 \pm 33^\circ\text{C}$  after (Nimis and Trommsdorff, 2001); 2.8 GPa  
893 and  $830^\circ\text{C}$  after (Hermann *et al.*, 2006)) are concordant with our new estimates. Hermann *et*  
894 *al.* (2006) provided also ~~P, T~~ estimates of ~~0.7-1.0 GPa and 720°C~~ for opx+sp+amph  
895 symplectites surrounding garnet. These ~~P, T~~ conditions are lower compared to our  
896 estimates on opx+cpx+sp, amph-free symplectites replacing garnet. ~~Thus,~~ they may refer to  
897 the post-granulitic, amphibolite-facies stage ~~that~~ we observed in both peridotite and mafic  
898 rocks. On the basis of U-Pb SHRIMP data on zircons found in amph-bearing symplectites,  
899 this stage occurred at 33-34 Ma and corresponds to the equilibration in the spinel peridotite  
900 field (Hermann *et al.*, 2006)..

Formattato: Tipo di carattere:  
Corsivo

Formattato: Tipo di carattere:  
Corsivo

Formattato: Tipo di carattere:  
Corsivo

Formattato: Tipo di carattere:  
Corsivo

Formattato: Tipo di carattere:  
Corsivo

901 Ky-bearing eclogites from the Duria area were only briefly acknowledged by Heinrich  
902 (1986), but no evidence of high-temperature, post-eclogitic overprint was reported. However,  
903 the author stressed out that the eclogites from the southern Adula Nappe record an eclogite-  
904 facies peak characterized by higher pressure and temperatures (c.  $800^\circ\text{C}$  and 2.4 GPa)  
905 compared to northern Adula ( $500^\circ\text{C}$  and 1.2 GPa).

906 Plagioclase + spinel coronas replacing kyanite have been reported by (Brouwer *et al.*,  
907 2005) in eclogites from Borgoglio in Onsernone Valley, ~~ca.~~ 50 km west from Monte Duria.  
908 However, ~~the~~ authors do not claim a post-eclogitic high-temperature event for these rocks,  
909 which are thought to have ~~re~~equilibrated at  $\sim 630^\circ\text{C}$  and 0.6 GPa during regional Barrovian  
910 metamorphism. Plagioclase + spinel + corundum symplectites after kyanite were described in  
911 eclogite-amphibolites from Gorduno/Alpe Arami (~~ca.~~ 15 km W from Mt Duria) by

912 (Brouwer, 2000), but the author did not provide P, ~~T~~, T constraints for symplectite formation,  
913 suggesting ~~T~~, T < 1050°C on the basis of the absence of sapphirine. In fact, except in  
914 eclogites from Duria described in our study, sapphirine was never observed in symplectites in  
915 eclogites from the Central Alps. However, sapphirine occurs as a rock-forming phase and as a  
916 symplectite constituent in granulites and charnokites from the Gruf Complex in Val Codera  
917 (Barker, 1964; Galli *et al.*, 2011), ~ 20 km ENE from Monte Duria (Fig. 1). In these rocks,  
918 Permian in age, sapphirine occurs with opx, cordierite, gt, sillimanite and corundum,  
919 suggesting ~~T~~, T > 900°C and ~~P~~, P = 0.85-0.95 GPa (Galli *et al.*, 2011). The high temperatures  
920 attained in the Gruf Complex has been considered so far an unique evidence for UHT  
921 metamorphism in the Central Alps.

Formattato: Tipo di carattere:  
Corsivo

Formattato: Tipo di carattere:  
Corsivo

Formattato: Tipo di carattere:  
Corsivo

Formattato: Tipo di carattere:  
Corsivo

922 Other significant occurrences of UHT metamorphism overprinting eclogite-facies rocks  
923 are reported from the Rhodope massif and various localities of the Variscan basement in  
924 Europe. Plagioclase ± sapphirine ± corundum ± spinel symplectites have been described in  
925 retrogressed eclogites from the central Rhodope in Greece (Liatì and Seidel, 1996), and  
926 estimated ~~P~~, ~~T~~, T conditions for the granulite facies were T > 800°C and ~~P~~, P > 1.5 GPa.

Formattato: Tipo di carattere:  
Corsivo

Formattato: Tipo di carattere:  
Corsivo

Formattato: Tipo di carattere:  
Corsivo

927 Discussing Rhodope granulitized eclogites, the authors stressed out that kyanite eclogites  
928 overprinted under granulite-facies conditions are known from the Variscan basement in  
929 Europe but not from the eclogites of Alpine age (cf. also Galli *et al.*, 2011), voicing the  
930 suspicion that these rocks could belong to a separate (pre-Alpine) tectonic unit. It should be  
931 noted, however, that this high-T granulite-facies metamorphism in central Rhodope was later  
932 questioned by (Moulas *et al.*, 2013). Nevertheless, similar sapphirine-bearing symplectites  
933 overprinting eclogite phases have been described in Variscan units in Europe, for instance:  
934 i) Armorican Massif, France (Godard and Mabit, 1998); ii) Bohemian Massif, Moldanubian  
935 zone, Austria ((Carswell *et al.*, 1989; Faryad *et al.*, 2006; O'Brien, 1997); iii) Golfo Aranci,  
936 Sardinia, Italy (Franceschelli *et al.*, 2007; Giacomini *et al.*, 2005); iv) Lotru Metamorphic  
937 Suite, South Carpatians (Săbău *et al.*, 2002); v) Pohorje, Eastern Alps, Slovenia (Vrabc *et al.*,  
938 2012).

939 Although new pressure and temperature estimated for the eclogite-facies peak in the  
940 Duria area are consistent with previous estimates concerning the Central Alps, in particular  
941 with garnet peridotites (e.g., Nimis & Trommsdorff, 2001) and eclogites (Brouwer *et al.*,  
942 2005) cropping out at Alpe Arami in the Southern Adula Nappe, a post-eclogite, high-  
943 temperature overprint involving ultramafic and mafic rocks has been never reported so far in  
944 Central Alps. Peridotites and eclogites from the Southern Adula display Alpine ages (Becker,  
945 1993; Brouwer *et al.*, 2005; Gebauer, 1996; Gebauer *et al.*, 1992). However, pre-Alpine high-

946 pressure metamorphic events have been dated by Liati et al. (2009) at 330-340 Ma in the  
947 northern and c. 370 Ma in the middle Adula. Moreover, (Herwartz *et al.*, 2011) report the case  
948 of an eclogite of the Central Adula (Trescolmen) showing two distinct age populations, being  
949 the older Variscan (332.7 Ma) and the younger Alpine (38 Ma). Therefore, these authors  
950 suggested that Trescolmen eclogite was subducted during Variscan orogeny and, later, it has  
951 been subducted again during the Alpine orogeny. Variscan eclogite-facies rocks, namely  
952 garnet peridotite and eclogite, dated back to ~330 Ma (Tumiati *et al.*, 2003, 2007) are known  
953 also in the Ulten zone (Eastern Alps; 150 km ENE from Duria). Pre-Alpine, low-P, high-T  
954 metamorphism has been evidenced in Central Alps in some rocks from the Gruf Complex,  
955 hosted in migmatites and characterized by UHT dated back to 282-260 Ma, followed by  
956 Alpine (34-29 Ma) amphibolite-facies metamorphism at 720-740°C and 0.65-0.75 GPa (Galli  
957 *et al.*, 2013, 2011). The latter P, ~~T~~, T conditions and ages are similar to those retrieved by  
958 Hermann *et al.* (2006) from amphibole-bearing symplectites in retrogressed garnet peridotites  
959 of Duria area. This LP-HT stage overprinting eclogite-facies rocks has never been reported  
960 before in the Adula-Cima Lunga nappe. Our new data add one more piece to the puzzle of the  
961 Central Alps, where Variscan and Alpine geodynamics interplayed, complicating the effort of  
962 deciphering the age and tectonometamorphic evolution of each unit (Biino *et al.*, 1997;  
963 Brueckner, 2011; Liati *et al.*, 2009).

964  
965 ~~Our new low P, high T conditions estimated for the post-eclogitic peak suggest that a re-~~  
966 ~~evaluation of the subduction-exhumation history and likely also of the age of pressure peak in~~  
967 ~~garnet peridotites and eclogites of Duria are needed.~~

## 969 CONCLUSIONS

970 Eclogite-facies rocks from Duria (Central Alps) share a common low-pressure, high-  
971 temperature metamorphic event at c. 1 GPa and 850-900°C. The metamorphic conditions and  
972 the petrological processes ~~recorded by~~ occurred in these rocks have been addressed by  
973 performing conventional thermobarometry and complex thermodynamic forward modelling  
974 of granulite-facies reactions involving Zr-bearing phases in peridotites and the high-pressure  
975 minerals kyanite and zoisite in eclogites, resulting in spinel ± sapphirine ± corundum  
976 symplectites. We ~~have readily~~ modelled the LP-HT mineral assemblages characterising these  
977 rocks by:

Formattato: Tipo di carattere:  
Corsivo

978 i) developing and integrating a new solid-solution model between  $ZrO_2$  and  $TiO_2$  with the  
979 intermediate compound srilankite  $(Zr, Ti)_2O_4$ , calibrated against previously published high-  
980 pressure experimental data.

981 ii) performing a material-transfer study using extensive properties, as the amount of poorly  
982 mobile chemical components, rather than intensive properties (i.e., chemical potentials),  
983 which are suitable only for perfectly mobile components.

984 ~~This LP-HT stage overprinting eclogite facies rocks has never been reported before in the~~  
985 ~~Adula-Cima Lunga nappe. Our new data add one more piece to the puzzle of the Central~~  
986 ~~Alps, where Variscan and Alpine geodynamics interplayed, complicating the effort of~~  
987 ~~deciphering the age and tectonometamorphic evolution of each unit (Biino *et al.*, 1997;~~  
988 ~~Brueckner, 2011; Liati *et al.*, 2009)). Our new low-P, high-T conditions estimated for the post-~~  
989 ~~eclogitic peak suggest that a re-evaluation of the subduction-exhumation history and likely~~  
990 ~~also of the age of pressure-peak in garnet peridotites and eclogites of Duria are needed.~~

991

992

#### 993 FUNDING

994 This work was supported by Italian Ministry of University and Research, [PRIN-  
995 2012R33ECR]. This work also benefited from the University of Milano Bicocca FAR12/13  
996 (12-1-2009100-139) and 2015-ATE-14440.

997

#### 998 ACKNOWLEDGEMENTS

999 [G. Godard, P. Nimis and an anonymous review, the editor J. Hermann](#)

1000 We thank Andrea Risplendente for the assistance at the scanning electron microscope and  
1001 electron microprobe. Discussion with J. Hermann and S. Poli helped to improve the  
1002 manuscript.

1003

#### 1004 REFERENCES:

1005

1006 Baldwin, J. a., Powell, R., Williams, M. L. & Goncalves, P. (2007). Formation of eclogite,  
1007 and reaction during exhumation to mid-crustal levels, Snowbird tectonic zone, western  
1008 Canadian Shield. *Journal of Metamorphic Geology* **25**, 953–973.

1009 Becker, H. (1993). Garnet peridotite and eclogite Sm-Nd mineral ages from the Lepontine  
1010 dome (Swiss Alps): New evidence for Eocene high-pressure metamorphism in the  
1011 central Alps. *Geology* **21**, 599.

- 1012 Berger, A., Burri, T., Alt-Epping, P. & Engi, M. (2008). Tectonically controlled fluid flow  
1013 and water-assisted melting in the middle crust: an example from the Central Alps. *Lithos*  
1014 **102**, 598–615.
- 1015 Berger, A., Mercolli, I. & Engi, M. (2005). The central Lepontine Alps: notes accompanying  
1016 the tectonicpetrographic map sheet Sopra Ceneri (1:100 000). *Schweizerische*  
1017 *Mineralogische Und Petrographische Mitteilungen* **85**, 109–146.
- 1018 Biino, G. G., Marquer, D. & Nussbaum, C. (1997). Alpine and pre-Alpine subduction events  
1019 in polycyclic basements of the Swiss Alps. *Geology* **25**, 751.
- 1020 Bingen, B., Austrheim, H. & Whitehouse, M. (2001). Ilmenite as a Source for Zirconium  
1021 during High-grade Metamorphism? Textural Evidence from the Caledonides of Western  
1022 Norway and Implications for Zircon Geochronology. *Journal of Petrology* **42**, 355–375.
- 1023 Brouwer, F. M. (2000). Thermal Evolution of High-Pressure Metamorphic Rocks in the Alps.  
1024 Utrecht University.
- 1025 Brouwer, F. M., Burri, T., Engi, M. & Berger, a (2005). Eclogite relics in the Central Alps:  
1026 PT-evolution, Lu-Hf ages and implications for formation of tectonic melange zones.  
1027 *Schweizerische Mineralogische Und Petrographische Mitteilungen* **85**, 147–174.
- 1028 Brueckner, H. K. (2011). Geodynamics: Double-dunk tectonics. *Nature Geoscience*. Nature  
1029 Publishing Group **4**, 136–138.
- 1030 Burri, T., Berger, a & Engi, M. (2005). Tertiary migmatites in the Central Alps: Regional  
1031 distribution, field relations, conditions of formation, and tectonic implications.  
1032 *Schweizerische Mineralogische Und Petrographische Mitteilungen* **85**, 215–232.
- 1033 Cancarevic, M., Zinkevich, M. & Aldinger, F. (2006). Thermodynamic Assessment of the  
1034 PZT System. *Journal of the Ceramic Society of Japan* **114**, 937–949.
- 1035 Carswell, D. A., Moller, C. & O'Brien, P. J. (1989). Origin of sapphirine-plagioclase  
1036 symplectites in metabasites from Mitterbachgraben, Dunkelsteinerwald granulite  
1037 complex, Lower Austria . *Eur. Journal Mineral* **1**, 455–466.
- 1038 Ciancaleoni, L. & Marquer, D. (2006). Syn-extension leucogranite deformation during  
1039 convergence in the Eastern Central Alps: example of the Novate intrusion. *Terra Nova*  
1040 **18**, 170–180.
- 1041 Connolly, J. a D. (2005). Computation of phase equilibria by linear programming: A tool for  
1042 geodynamic modeling and its application to subduction zone decarbonation. *Earth and*  
1043 *Planetary Science Letters* **236**, 524–541.
- 1044 Dale, J. & Holland, T. J. B. (2003). Geothermobarometry, P-T paths and metamorphic field  
1045 gradients of high-pressure rocks from the Adula Nappe, Central Alps. *Journal of*

- 1046 *Metamorphic Geology* **21**, 813–829.
- 1047 Dale, J., Holland, T. & Powell, R. (2000). Hornblende–garnet–plagioclase thermobarometry:  
1048 a natural assemblage calibration of the thermodynamics of hornblende. *Contributions to*  
1049 *Mineralogy and Petrology*. Springer Berlin Heidelberg **140**, 353–362.
- 1050 Dewey, J. F., Helman, M. L., Knott, S. D., Turco, E. & Hutton, D. H. W. (1989). Kinematics  
1051 of the western Mediterranean. *Geological Society Special Publications* **45**, 265–283.
- 1052 DIENER, J. F. A. & POWELL, R. (2012). Revised activity-composition models for  
1053 clinopyroxene and amphibole. *Journal of Metamorphic Geology*. Blackwell Publishing  
1054 Ltd **30**, 131–142.
- 1055 Eckert, J. O., Newton, R. C. & Kleppa, O. J. (1991). The DH of reaction and recalibration of  
1056 garnet–pyroxene–plagioclase–quartz geo- barometers in the CMAS system by solution  
1057 calorimetry. *American Mineralogist* **76**, 148–160.
- 1058 Evans, B. W. & Trommsdorff, V. (1978). Petrogenesis of garnet lherzolite, Cima di Gagnone,  
1059 Lepontine Alps. *Earth and Planetary Science Letters* **40**, 333–348.
- 1060 Faryad, S. W., Perraki, M. & Vrána, S. (2006). P-T evolution and reaction textures in  
1061 retrogressed eclogites from Svetlik, the Moldanubian Zone (Czech Republic).  
1062 *Mineralogy and Petrology* **88**, 297–319.
- 1063 Franceschelli, M., Puxeddu, M., Cruciani, G. & Utzeri, D. (2007). Metabasites with eclogite  
1064 facies relics from Variscides in Sardinia, Italy: A review. *International Journal of Earth*  
1065 *Sciences* **96**, 795–815.
- 1066 Frey, M. & Ferreiro-Mählmann, R. (1999). Alpine metamorphism in the Central Alps.  
1067 *Schweizerische Mineralogische und Petrographische Mitteilungen* **79**, 135–154.
- 1068 Fumasoli, M. W. (1974). Geologie des Gebietes nördlich und südlich der Jorio-Tonale-Linie  
1069 im Westen von Gravedone (Como, Italia). Universität Zürich.
- 1070 Galli, A., Le Bayon, B., Schmidt, M. W., Burg, J. P. & Reusser, E. (2013).  
1071 Tectonometamorphic history of the Gruf complex (Central Alps): Exhumation of a  
1072 granulite-migmatite complex with the Bergell pluton. *Swiss Journal of Geosciences* **106**,  
1073 33–62.
- 1074 Galli, a., Le Bayon, B., Schmidt, M. W., Burg, J. P., Caddick, M. J. & Reusser, E. (2011).  
1075 Granulites and charnockites of the Gruf Complex: Evidence for Permian ultra-high  
1076 temperature metamorphism in the Central Alps. *Lithos*. Elsevier B.V. **124**, 17–45.
- 1077 Galster, F., Cavargna-Sani, M., Epard, J. & Masson, H. (2012). New stratigraphic data from  
1078 the Lower Penninic between the Adula nappe and the Gotthard massif and consequences  
1079 for the tectonics and the paleogeography of the Central Alps. *Tectonophysics* **579**, 37–



1080 55.

1081 Gebauer, D. (1996). A P-T-t Path for an (Ultra?-) High-pressure Ultramafic/Mafic Rock-  
1082 Association and its Felsic Country-Rocks Based on SHRIMP-Dating of Magmatic and  
1083 Metamorphic Zircon Domains. Example: Alpe Arami (Central Swiss Alps). *Geophysical*  
1084 *Monograph Series* **95**, 307–329.

1085 Gebauer, D., Grunenfelder, M., Tilton, G., Trommsdorff, V. & Sschimd, S. (1992). The  
1086 geodynamic evolution of garnet-peridotites, garnet pyroxenites and eclogites of Alpe  
1087 Arami and Cima Gagnone (Central Alps) from Early Proterozoic to Oligocene. *Schweiz.*  
1088 *Min. Petr. Mitt.* **72**, 107–111.

1089 Giacomini, F., Bomparola, R. M. & Ghezzi, C. (2005). Petrology and geochronology of  
1090 metabasites with eclogite facies relics from NE Sardinia: Constraints for the Palaeozoic  
1091 evolution of Southern Europe. *Lithos* **82**, 221–248.

1092 Godard, G. & Mabit, J. L. (1998). Peraluminous sapphirine formed during retrogression of a  
1093 kyanite-bearing eclogite from Pays de Leon, Armorican Massif, France. *Lithos* **43**, 15–  
1094 29.

1095 Godard, G. & Martin, S. (2000). Petrogenesis of kelyphites in garnet peridotites: A case study  
1096 from the Ulten zone, Italian Alps. *Journal of Geodynamics* **30**, 117–145.

1097 Heinrich, C. A. (1986). Eclogite facies regional metamorphism of hydrous mafic rocks in the  
1098 Central Alpine Adula nappe. *Journal of Petrology* **27**, 123–154.

1099 Hermann, J., Rubatto, D. & Trommsdorff, V. (2006). Sub-solidus Oligocene zircon formation  
1100 in garnet peridotite during fast decompression and fluid infiltration (Duria, Central  
1101 Alps). *Mineralogy and Petrology* **88**, 181–206.

1102 Herwartz, D., Nagel, T. J., Münker, C., Scherer, E. E. & Fritzsche, N. (2011). Tracing two  
1103 orogenic cycles in one eclogite sample by Lu–Hf garnet chronometry. *Nature*  
1104 *Geoscience*. Nature Publishing Group **4**, 178–183.

1105 Holland, T. (1980). The reaction albite = jadeite + quartz determined experimentally in the  
1106 range 600–1200.c. *American Mineralogist* **65**, 129–134.

1107 Holland, T. J. B. & Powell, R. (1998). An internally consistent thermodynamic data set for  
1108 phases of petrological interest. *Journal of Metamorphic Geology* **16**, 309–343.

1109 Holland, T. & Powell, R. (2003). Activity–composition relations for phases in petrological  
1110 calculations: an asymmetric multicomponent formulation. *Contributions to Mineralogy*  
1111 *and Petrology*. Springer-Verlag **145**, 492–501.

1112 Johansson, L. & Möller, C. (1986). Formation of sapphirine during retrogression of a basaltic  
1113 high-pressure granulite, Roan, Western Gneiss Region, Norway. *Contributions to*

- 1114 *Mineralogy and Petrology* **94**, 29–41.
- 1115 Korzhinskii, D. S. (1959). *Physicochemical Basis of the Analysis of the Paragenesis of*  
1116 *Minerals*. New York: Consultants bureau, inc.
- 1117 Krogh Ravna, E. (2000). The garnet – clinopyroxene Fe<sup>2+</sup> – Mg geothermometer: an  
1118 updated calibration. *Journal of Metamorphic Geology* **18**, 211–219.
- 1119 Liati, A., Gebauer, D. & Fanning, C. M. (2009). Geochronological evolution of HP  
1120 metamorphic rocks of the Adula nappe, Central Alps, in pre-Alpine and Alpine  
1121 subduction cycles. *Journal of the Geological Society* **166**, 797–810.
- 1122 Liati, A. & Seidel, E. (1996). Metamorphic evolution and geochemistry of kyanite eclogites  
1123 in central Rhodope, northern Greece. *Contributions to Mineralogy and Petrology* **123**,  
1124 293–307.
- 1125 Milnes, A. G. (1974). Structure of the Pennine Zone (Central Alps): a new working  
1126 hypothesis. Bulletin of the Geological Society of America. *Bulletin of the Geological*  
1127 *Society of America* **85**, 1727–1732.
- 1128 Morishita, T., Arai, S. & Gervilla, F. (2001). High-pressure aluminous mafic rocks from the  
1129 Ronda peridotite massif, southern Spain: Significance of sapphirine- and corundum-  
1130 bearing mineral assemblages. *Lithos* **57**, 143–161.
- 1131 Morishita, T., Maeda, J., Miyashita, S., Matsumoto, T. & Dick, H. J. B. (2004). Magmatic  
1132 srilankite (Ti<sub>2</sub>ZrO<sub>6</sub>) in gabbroic vein cutting oceanic peridotites: An unusual product  
1133 of peridotite-melt interactions beneath slow-spreading ridges. *American Mineralogist* **89**,  
1134 759–766.
- 1135 Morten, L. & Trommsdorff, V. (2003). Metamorphism and textures of dry and hydrous garnet  
1136 peridotites. *EMU*, 443–466.
- 1137 Moulas, E., Kostopoulos, D., Connolly, J. A. D. & Burg, J. P. (2013). P-T estimates and  
1138 timing of the sapphirine-bearing metamorphic overprint in kyanite eclogites from  
1139 Central Rhodope, northern Greece. *Petrology* **21**, 507–521.
- 1140 Nagel, T. J. (2008). Tertiary subduction, collision and exhumation recorded in the Adula  
1141 nappe, central Alps. *Geological Society, London, Special Publications* **298**, 365–392.
- 1142 Nakamura, D. & Hirajima, T. (2000). Granulite-facies overprinting of ultrahigh-pressure  
1143 metamorphic rocks, northeastern Su-Lu region, eastern China. *Journal of Petrology* **41**,  
1144 563–582.
- 1145 Nimis, P. & Grütter, H. (2010). Internally consistent geothermometers for garnet peridotites  
1146 and pyroxenites. *Contributions to Mineralogy and Petrology* **159**, 411–427.

- 1147 Nimis, P. & Taylor, W. R. (2000). Single clinopyroxene thermobarometry for garnet  
1148 peridotites. Part I. Calibration and testing of a Cr-in-Cpx barometer and an enstatite-in-  
1149 Cpx thermometer. *Contributions to Mineralogy and Petrology*. Springer Berlin  
1150 Heidelberg **139**, 541–554.
- 1151 Nimis, P. & Trommsdorff, V. (2001). Revised Thermobarometry of Alpe Arami and other  
1152 Garnet Peridotites from the Central Alps. *Journal of Petrology* **42**, 103–115.
- 1153 O'Brien, P. J. (1997). Garnet zoning and reaction textures in overprinted eclogites, Bohemian  
1154 Massif, European variscides: a record of their thermal history during exhumation. *Lithos*  
1155 **41**, 119–133.
- 1156 O'Neill, H. S. C. (1981). The transition between spinel lherzolites and garnet lherzolites, and  
1157 its use as a geobarometer. *Contributions to Mineralogy and Petrology* **77**, 185–194.
- 1158 Pfiffner, M. & Trommsdorff, V. (1998). The high-pressure ultramafic-mafic-carbonate suite  
1159 of Cima Lunga-Adula, Central Alps: Excursions to Cima di Gagnone and Alpe Arami.  
1160 *Schweizerische Mineralogische und Petrographische Mitteilungen* **78**, 337–354.
- 1161 Ravna, E. J. K. & Terry, M. P. (2004). Geothermobarometry of UHP and HP eclogites and  
1162 schists - An evaluation of equilibria among garnet-clinopyroxene-kyanite-phengite-  
1163 coesite/quartz. *Journal of Metamorphic Geology* **22**, 579–592.
- 1164 Rubatto, D., Hermann, J., Berger, A. & Engi, M. (2009). Protracted fluid-present melting  
1165 during Barrovian metamorphism in the Central Alps. *Contributions to Mineralogy and*  
1166 *Petrology* **158**, 703–722.
- 1167 Săbău, G., Alberico, A. & Negulescu, E. (2002). Peraluminous Sapphirine in Retrogressed  
1168 Kyanite-bearing Eclogites from the South Carpathians: Status and Implications.  
1169 *International Geology Review* **44**, 859–876.
- 1170 Sato, K., Miyamoto, T. & Kawasaki, T. (2006). Experimental Calibration of Sapphirine-  
1171 Spinel Fe<sup>2+</sup>-Mg Exchange Thermometer: Implication for Constraints on P-T Condition  
1172 of Howard Hills, Napier Complex, East Antarctica. *Gondwana Research* **9**, 398–408.
- 1173 Schmid, S. M., O.A., P., Froitzheim, N., Schönborn, G. & Kissinger, E. (1996). Geophysical-  
1174 geological transect and tectonic evolution of the Swiss-Italian Alps. *Tectonics* **15**, 1036–  
1175 1064.
- 1176 Schmidt, M. W. & Poli, S. (1998). Experimentally based water budgets for dehydrating slabs  
1177 and consequences for arc magma generation. *Earth and Planetary Science Letters* **163**,  
1178 361–379.
- 1179 Scott, J. M., Konrad-Schmolke, M., O'Brien, P. J. & Günter, C. (2013). High-T, low-P  
1180 formation of rare olivine-bearing symplectites in variscan eclogite. *Journal of Petrology*

1181           **54**, 1375–1398.

1182 Skjerlie, K. P. & Patino Douce, A. E. (2002). The Fluid-absent Partial Melting of a Zoisite-  
1183 bearing Quartz Eclogite from 1{middle dot}0 to 3{middle dot}2 GPa; Implications for  
1184 Melting in Thickened Continental Crust and for Subduction-zone Processes. *J. Petrology*  
1185 **43**, 291–314.

1186 Steinmann, M. & Stille, P. (1999). Geochemical evidence for the nature of the crust beneath  
1187 the eastern North Penninic basin of the Mesozoic Tethys ocean. *Geologische Rundschau*  
1188 **87**, 633–643.

1189 Stucki, A., Rubatto, D. & Trommsdorff, V. (2003). Mesozoic ophiolite relics in the Southern  
1190 Steep Belt of the Central Alps. *Schweizerische Mineralogische und Petrographische*  
1191 *Mitteilungen* **83**, 285–299.

1192 Taylor, W. R. (1998). An experimental test of some geothermometer and geobarometer  
1193 formulations for upper mantle peridotites with application to the thermobarometry of  
1194 fertile lherzolite and garnet websterite. *Neues Jahrbuch für Mineralogie, Abhandlungen*  
1195 **172**, 381–408.

1196 Todd, C. S. & Engi, M. (1997). No Title. *Metamorphic field gradients in the Central Alps.*  
1197 *Journal of Metamorphic Geology* **15**, 513–530.

1198 TOMKINS, H. S., POWELL, R. & Ellis, D. J. (2007). The pressure dependence of the  
1199 zirconium-in-rutile thermometer. *Journal of Metamorphic Geology*. Blackwell  
1200 Publishing Ltd **25**, 703–713.

1201 Troitzsch, U., Christy, A. G. & Ellis, D. J. (2004). Synthesis of ordered zirconium titanate  
1202 (Zr,Ti)<sub>2</sub>O<sub>4</sub> from the oxides using fluxes. *Journal of the American Ceramic Society* **87**,  
1203 2058–2063.

1204 Troitzsch, U. & Ellis, D. J. (2004). High-PT study of solid solutions in the system  
1205 ZrO<sub>2</sub>-TiO<sub>2</sub>: The stability of srilankite. *European*  
1206 *Journal of Mineralogy* **16**, 577–584.

1207 Tumiati, S., Godard, G., Martin, S., Klötzli, U. & Monticelli, D. (2007). Fluid-controlled  
1208 crustal metasomatism within a high-pressure subducted mélangé (Mt. Hochwart, Eastern  
1209 Italian Alps). *Lithos* **94**, 148–167.

1210 Tumiati, S., Godard, G., Martin, S., Malaspina, N. & Poli, S. (2015). Lithos Ultra-oxidized  
1211 rocks in subduction mélanges: Decoupling between oxygen fugacity and oxygen  
1212 availability in a Mn-rich metasomatic environment. *LITHOS*. Elsevier B.V.

1213 Tumiati, S., Thöni, M., Nimis, P., Martin, S. & Mair, V. (2003). Mantle-crust interactions  
1214 during Variscan subduction in the Eastern Alps (Nonsberg-Ulten zone): Geochronology

1215 and new petrological constraints. *Earth and Planetary Science Letters* **210**, 509–526.

1216 Vrabec, M., Janák, M., Froitzheim, N. & De Hoog, J. C. M. (2012). Phase relations during  
1217 peak metamorphism and decompression of the UHP kyanite eclogites, Pohorje  
1218 Mountains (Eastern Alps, Slovenia). *Lithos*. Elsevier B.V. **144–145**, 40–55.

1219 Wang, L., Essene, E. J. & Zhang, Y. (1999). Mineral inclusions in pyrope crystals from  
1220 Garnet Ridge, Arizona, USA: Implications for processes in the upper mantle.  
1221 *Contributions to Mineralogy and Petrology* **135**, 164–178.

1222 Wenk, E. (1970). Zur Regionalmetamorphose und Ultrametamorphose der Zentralalpen.  
1223 *Fortschritte der Mineralogie* **47**, 555–565.

1224 Zack, T., Moraes, R. & Kronz, a. (2004). Temperature dependence of Zr in rutile: Empirical  
1225 calibration of a rutile thermometer. *Contributions to Mineralogy and Petrology* **148**,  
1226 471–488.

1227

## 1228 TABLES

1229

1230 Table 1: Bulk-rock composition of selected samples from Duria. All rocks were sampled at  
1231 the outcrop of Borgo (Figs. 1, 2), with the exception of garnet peridotite A2C2 (Monte Duria).

1232

1233 Table 2: Representative microprobe analyses of olivine (Ol), clinopyroxene (Cpx), and  
1234 orthopyroxene (Opx) in selected samples (see Table 1). Fine: fine-grained; C: core; R: rim;  
1235 InGt: included in garnet; InCpx: included in clinopyroxene; Sym: in symplectite. Fe<sup>2+</sup> and  
1236 Fe<sup>3+</sup> are calculated from stoichiometry.

1237

1238 Table 3: Representative microprobe analyses of garnet (Gt), amphibole (Amp), spinel (Sp),  
1239 sapphirine (Sapp), plagioclase (Pl) and phlogopite (Bt) in selected peridotite and eclogite  
1240 samples from Duria (see Table 1). Fine: fine-grained; C: core; R: rim; Sym: in symplectite.  
1241 Fe<sup>2+</sup> and Fe<sup>3+</sup> are calculated from stoichiometry.

1242

## 1243 FIGURES

1244

1245 Figure 1. (a) Tectonic scheme of the Lepontine Dome in the Central Alps. Isotherms of the  
1246 post nappe-stacking barrovian metamorphic event and the extent of the migmatite belt are  
1247 from Todd and Engi (1997) and Burri *et al.* (2005), respectively. (b) Detailed geological

1248 scheme of the Duria area with the locations of Monte Duria and Borgo outcrops. Main  
1249 geological features are modified from Berger *et al.* (2005).

1250

1251 | Figure 2. [Form surface mapping](#) Map of the Borgo outcrop along the Ledù stream. AG:  
1252 amphibolic migmatitic gneiss; E: kyanite eclogites; HAE: high-Al<sub>2</sub>O<sub>3</sub> rim between kyanite  
1253 eclogites and hosting amphibole-bearing migmatitic gneiss; ME: mafic eclogites; MG:  
1254 | migmatitic gneiss; OGN: orthogneiss; PDT: retrogressed garnet peridotite. ~~(a)~~

1255

1256 Figure 3. Field aspect of peridotite lenses at Borgo (a, b, c, d, e, f) and Monte Duria (g, h).

1257 (a) Loose block of partially retrogressed garnet peridotite downstream of the Borgo outcrop;  
1258 | (b) compositional layering made by garnet-rich and [garnet-garnet](#)-poor layers in the Borgo  
1259 | peridotite.; a pervasive chlorite-[defined](#) foliation overprinting the layering occurs within 4–5  
1260 m from the contact with hosting crustal rocks; (c) a boudin of mafic eclogite (ME) within  
1261 | amphibole-bearing migmatitic gneiss (AG); (d) a large (ca. 7 m x 5 m) boudin of kyanite  
1262 eclogite (E); (e) detail of the contact between kyanite eclogite and hosting gneiss with the red-  
1263 to pink-coloured Al<sub>2</sub>O<sub>3</sub>-rich rim (HAE); (f) emerald green zoisite crystal within the HAE rim;  
1264 | (g) peridotite lens on the SE ridge of Monte Duria (L. [Pellegrino](#) for scale): garnet  
1265 porphyroclasts are preserved only at cores, whereas a chlorite foliation, associated to the  
1266 retrogression in the spinel stability field occurs on the outer rim; (h) detail of anhedral to sub-  
1267 | euhedral garnet porphyroclasts with dark-coloured thin [symplectitic-kelyphitic](#) rims.

1268

1269 | Figure 4. [Representative transmitted light p](#)hotomicrographs of Duria rocks: (a) peridotite  
1270 sample B3A showing garnet porphyroclast (gt) surrounded by kelyphite, in a matrix of  
1271 fractured olivine (ol); (b) detail of the olivine matrix showing a porphyroclast of  
1272 orthopyroxene (opx); (c) detail of a double corona surrounding garnet, with secondary  
1273 orthopyroxene developing towards olivine and kelyphite towards garnet.; (d) kyanite  
1274 porphyroclast (ky) in eclogite sample B5, surrounded by symplectite and a plagioclase corona  
1275 (pl) towards the host symplectitic matrix; (e, f) parallel- and crossed-polarised light  
1276 micrographs showing the symplectitic matrix of sample B5, with garnet (gt), kyanite (ky) and  
1277 amphibole (amp) porphyroclasts; (g) mafic eclogite D6, showing garnet porphyroclasts (gt)  
1278 embedded in a symplectitic matrix; (h) zoisite porphyroclast (zo) replaced by symplectite in  
1279 high-Al<sub>2</sub>O<sub>3</sub> eclogite sample D1.

1280

1281 Figure 5. Back-scattered electron (BSE) images of Duria rocks: (a) olivine (ol) in former  
1282 contact with garnet (out of sight) surrounded by a double corona consisting of orthopyroxene  
1283 (opx) in the inner part, and orthopyroxene (opx) + clinopyroxene (cpx) and spinel (sp) in the  
1284 outer part; apatite (ap), zircon (zrc), baddeleyite (bdy) and srilankite (sril) occur in textural  
1285 equilibrium the coronitic assemblages (sample A2C2); (b) overview of garnet (gt) in former  
1286 contact with olivine (ol), replaced by opx+cpx+sp kelyphite; olivine is replaced by secondary  
1287 orthopyroxene (opx); Cr-rich spinel (Cr-sp) and clinopyroxene (cpx) porphyroclasts occur in  
1288 the peridotite matrix (sample B1); (c) mineral assemblages in eclogite B5, showing kyanite  
1289 (ky), garnet (gt), amphibole (amp) and quartz (q) porphyroclasts embedded in a symplectitic  
1290 intergrowth of clinopyroxene (cpx) and plagioclase (pl). Coronitic assemblages are  
1291 plagioclase + amphibole surrounding relict garnet and plagioclase + spinel (sp) + sapphirine  
1292 (sapp) replacing kyanite; (d) relict omphacite (omph) in kyanite porphyroclast replaced by  
1293 pl+sp sumplectite (sample B5); (e) relict coronitic assemblage pl+orthopyroxene (opx)  
1294 replacing garnet in mafic eclogite D6; (f) K-feldspar porphyroclasts in mafic eclogite D6; (g)  
1295 zoisite porphyroclast replaced by a corona of plagioclase in the inner part and a pl +  
1296 corundum (cor) + sapp + sp symplectite in the outer part towards the eclogite matrix (sample  
1297 D1); (h) kyanite porphyroclast completely replaced by a composite symplectite, ~~cor-rich in~~  
1298 ~~the core, pl-rich in the rim and sp+sapp-bearing in the middle~~-(sample D9).

1300 Figure 6. Principal component analysis of the bulk-rock compositions shown in Table 1.  
1301 Kyanite-eclogites (E) B5 and D3 display the lowest ~~absolute eigenvalues-F1-F2 coordinates~~  
1302 and their composition can be considered the reference point for eclogites outcropping at  
1303 Borgo. Mafic eclogites (ME) D4 and D6 display the highest ~~value-coordinate~~ for the principal  
1304 component F1, which represent the relative enrichment of Fe, Mn, Ti and P. The high-Al<sub>2</sub>O<sub>3</sub>  
1305 ~~eclogites (HAE) D1, B8 and D9 are characterised by the lowest F1 value-coordinate, being~~  
1306 ~~enriched-rich~~ in Al<sub>2</sub>O<sub>3</sub> and SiO<sub>2</sub>, while the retrogressed amphibole-gneisses (AG) D2 and D5  
1307 show relatively high contents in CaO and MgO.

1309 Figure 7. Conventional thermobarometry of Duria peridotites. HP, LP: calculations performed  
1310 using the compositions of the phases belonging to the high-pressure and low-pressure  
1311 assemblages, respectively. NG: Nimis and Grütter, 2010; Ta: Taylor, 1998; BK: Brey and  
1312 Köhler, 1990; O'N81: O'Neill (1981). Further details provided in text.

1313

1314 Figure 8. Thermodynamic modelling of Zr-bearing symplectites. (a) Binary  $ZrO_2$ - $TiO_2$  T-X  
1315 diagram calculated at fixed  $P, P = 2.0$  GPa using the *Perple\_X* package  
1316 (<http://www.perplex.ethz.ch>) and a new baddeleyite-rutile solid-solution model calibrated  
1317 against the experimental data of Troitzsch et al. (2004) (red dots). Activity-composition  
1318 relations among baddeleyite, rutile and srilankite are retrieved using the van Laar formulation  
1319 (Holland and Powell, 2003), which allows describing asymmetrical miscibility gaps ( $\alpha_{bdy}$   
1320 0.35, 0.000546, 0.0;  $\alpha_{srl}$  1.1, 0.0, 0.0;  $\alpha_{ru}$  0.7, 0.0, 0.0); (b) Calculated P-T diagram showing  
1321 the univariant srilankite-in reaction forsterite + rutile + zircon = srilankite + enstatite in the  
1322 system  $MSMgO+SiO_2+TiO_2+ZrO_2$ . Ternary  $SiO_2$ - $TiO_2$ - $ZrO_2$  chemographies (forsterite  
1323 always in excess) are calculated at  $T < T_{srl}$  and  $T > T_{srl}$ . Rutile-  
1324 enriched (blue star) and zircon-enriched (green star) bulk compositions are shown for  
1325 reference; (c, d) P,  $T$  pseudosections in the system  $CFMAS+TiO_2+ZrO_2$  calculated for a  
1326 fixed bulk composition corresponding to 1 mol garnet + 1 mol olivine, with components  $TiO_2$   
1327 and  $ZrO_2$  added in minor amounts with  $X_{Ti} (=TiO_2/ZrO_2+TiO_2) = 0.75$  in (c) and 0.25 in (d);  
1328 the srilankite-in reaction in the MS-  $TiO_2+ZrO_2$  is shown for reference as dashed line.

1329  
1330 Figure 9. Conventional thermobarometry of Duria eclogites. (a) blue lines: clinopyroxene-  
1331 garnet thermometer after Krogh (2000) and jadeite-in-clinopyroxene barometer after Holland  
1332 (1980); green shaded field: range of temperatures retrieved using the Zr-in-rutile thermometer  
1333 of Tomkins et al. (2007); red dashed line: Ti-in-quartz thermometer of Wark and Watson  
1334 (2006); grey dashed lines: experimental amp- and zo-out from Schmidt and Poli (1998), and  
1335 coesite-quartz transition; (b) blue lines: Ca-in-orthopyroxene thermometer of Brey and Köhler  
1336 (1990) and barometers of Lal (1993) (gt-opx-pl-q) and Eckert et al. (1991) (gt-cpx-pl-q);  
1337 green line: sapphirine-spinel thermometer of Sato et al. (2006); grey dashed lines:  
1338 experimental wet solidus and garnet-in from Schmidt and Poli (1998).

1339  
1340 Figure 10. Thermodynamic modelling of E-type kyanite eclogites from Duria. (a) P-T  
1341 isochemical section calculated for the composition B5, assuming  $H_2O = 0.01$  wt%; isopleths  
1342 of the calculated molar fraction of the component  $KAlSi_3O_8$  in K-feldspar (X<sub>Or</sub>) are shown as  
1343 dotted lines; the experimental wet solidus of Schmidt and Poli (1998) is shown for  
1344 comparison as dashed line; (b) P-X isothermal section calculated at fixed  $T = 700^\circ C$ , where  
1345  $X = 0$  stands for the anhydrous bulk composition B5 and  $X = 1$  represents the composition  
1346 B5 with wt% added  $H_2O$  component.

Formattato: Tipo di carattere:  
Corsivo

Formattato: Pedice

Formattato: Tipo di carattere:  
Corsivo

Formattato: Tipo di carattere:  
Corsivo

Formattato: Tipo di carattere:  
Corsivo

Formattato: Tipo di carattere:  
Corsivo

Formattato: Evidenziato



1348 Figure 11. Thermodynamic modelling of symplectites replacing kyanite in E-type and HAE-  
1349 type eclogites from Durlia. (e, d) P-X isothermal sections calculated at fixed  $T, T = 850^{\circ}\text{C}$ ,  
1350 where  $X = 1$  represents composition B5 (c, E-type eclogites) or D9 (d, HAE-type eclogites)  
1351 with 0.01 wt% added  $\text{H}_2\text{O}$ , and  $X = 0$  accounts for 30 wt% added kyanite component  
1352  $\text{Al}_2\text{SiO}_5$ .

Formattato: Tipo di carattere:  
Corsivo

1354 Figure 12. Thermodynamic modelling of symplectites replacing zoisite in HAE-type eclogites  
1355 from Durlia (e) P-X isothermal section calculated at fixed  $T, T = 850^{\circ}\text{C}$ , where  $X = 1$   
1356 represents composition D1 with 0.01 wt% added  $\text{H}_2\text{O}$ , and  $X = 0$  accounts for 50 wt% added  
1357 zoisite component  $\text{CaAl}_2\text{Si}_2\text{O}_{12}(\text{OH})$ ; (f)  $\log a_{\text{H}_2\text{O}}$  vs. X section calculated at fixed  $P, P = 1.2$   
1358 GPa and  $T, T = 850^{\circ}\text{C}$ , where  $X = 1$  represents composition D1 with 0.01 wt% added  $\text{H}_2\text{O}$ ,  
1359 and  $X = 0$  accounts for 50 wt% added zoisite component  $\text{CaAl}_2\text{Si}_2\text{O}_{12}(\text{OH})$ .

Formattato: Evidenziato

Formattato: Tipo di carattere:  
Corsivo, Evidenziato

Formattato: Evidenziato

Formattato: Tipo di carattere:  
Corsivo, Evidenziato

Formattato: Evidenziato

Formattato: Tipo di carattere:  
Corsivo, Evidenziato

Formattato: Evidenziato

1361 Figure 13. Schematic cartoon showing symplectites replacing kyanite in type E eclogites (a,  
1362 b) and HAE eclogites (c, d) on the basis of the thermodynamic modelling and related  
1363 material-transfer study. (a) Former HP kyanite porphyroclast in kyanite eclogite B5 redrawn  
1364 from the BSE inset (detail of Fig. 5c), embedded in a matrix of omphacite and garnet; (b) LP-  
1365 HT reactions 4 ( $\text{ky} + \text{omph} + \text{gt} = \text{pl} + \text{sapp}$ ) and 5 ( $\text{ky} + \text{omph} + \text{gt} = \text{pl} + \text{sp}$ ) (see text) result  
1366 in symplectites made of An-rich plagioclase together with sapphirine (sapp; blue fields in  
1367 inset, cf. Fig. 11a) or spinel (sp; pink fields), depending on the amount of  $\text{Al}_2\text{SiO}_5$  (kyanite)  
1368 component added to the bulk rock. Compositional isopleths can be drawn in the symplectite  
1369 in order to reproduce the microstructure of the symplectite. (c, d) In eclogite D9, symplectite  
1370 replacing kyanite, shown in the inset (cf. Fig. 5h) contains corundum (cor) in its inner part  
1371 (green fields in inset, cf. Fig. 11b), due to reaction 6 ( $\text{ky} + \text{omph} = \text{cpx} + \text{pl} + \text{cor}$ ). Sapphirine  
1372 + corundum (grey fields), sapphirine + spinel (yellow fields) and spinel only (pink fields)  
1373 occur in symplectite towards the rock matrix. The observed microstructure can be modelled  
1374 perfectly assuming also in this case a decreasing amount of the component  $\text{Al}_2\text{SiO}_5$  from the  
1375 core to the rim in the micro-domain surrounding the kyanite crystal that has been replaced by  
1376 LP-HT mineral assemblages. Dashed red arrows in figures b and d indicates possible paths  
1377 from the  $\text{Al}_2\text{SiO}_5$ -rich symplectite core towards the host bulk-rock.